iScience

Article

Transcriptomic landscape of hyperthyroidism in mice overexpressing thyroid-Stimulating hormone

Graphical abstract

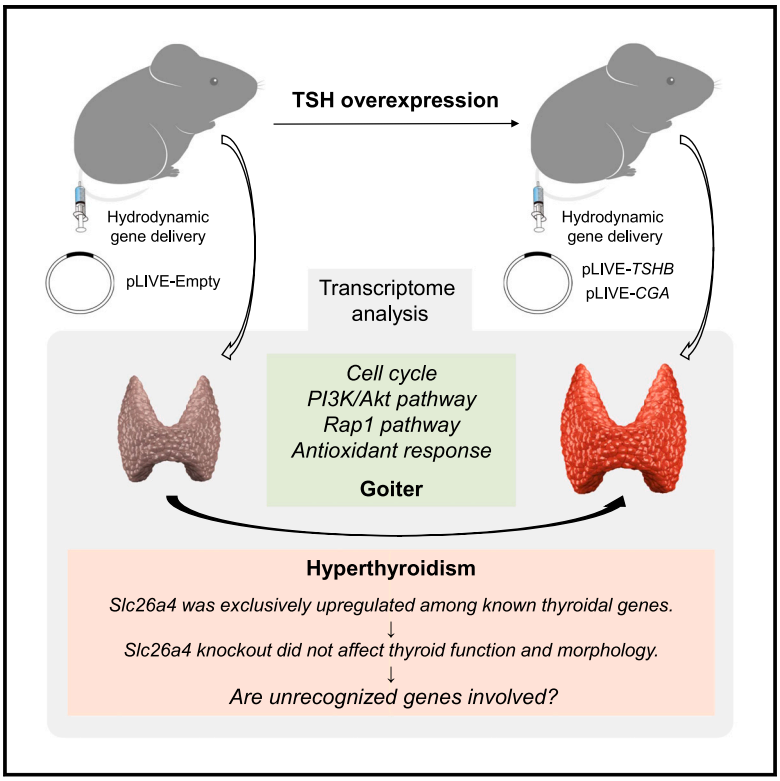

Highlights

- We generated mice overexpressing thyroid-stimulating hormone (TSH) via gene delivery
- These mice exhibited hyperthyroidism and goiters
- TSH overexpression drastically changed their thyroid transcriptome
- Our transcriptome datasets can contribute to future research on hyperthyroidism

Authors

Ichiro Yamauchi, Taku Sugawa, Takuro Hakata, ..., Yoriko Sakane, Akihiro Yasoda, Nobuya Inagaki

Correspondence

ichiroy@kuhp.kyoto-u.ac.jp

In brief

Endocrine system physiology; Endocrinology; Transcriptomics; Model organism

Yamauchi et al., 2025, iScience *28*, 111565
January 17, 2025
https://doi.org/10.1016/j.isci.2024.111565

CellPress

iScience

CellPress
OPEN ACCESS

Article

Transcriptomic landscape of hyperthyroidism in mice overexpressing thyroid-Stimulating hormone

Ichiro Yamauchi,[1,6,*] Taku Sugawa,[1] Takuro Hakata,[1] Akira Yoshizawa,[2] Tomoko Kita,[2] Yo Kishimoto,[2] Sadahito Kimura,[1] Aya Sakurai,[1] Daisuke Kosugi,[1] Haruka Fujita,[1] Kentaro Okamoto,[1] Yohei Ueda,[1] Toshihito Fujii,[1] Daisuke Taura,[1] Yoriko Sakane,[1,3] Akihiro Yasoda,[4] and Nobuya Inagaki[5]

[1]Department of Diabetes, Endocrinology and Nutrition, Graduate School of Medicine, Kyoto University, Sakyo-ku, Kyoto 606-8507, Japan
[2]Department of Otolaryngology-Head and Neck Surgery, Graduate School of Medicine, Kyoto University, Sakyo-ku, Kyoto 606-8507, Japan
[3]Sugawa Clinic, Nakagyo-ku, Kyoto 604-8105, Japan
[4]Clinical Research Center, National Hospital Organization Kyoto Medical Center, Fushimi-ku, Kyoto 612-8555, Japan
[5]Medical Research Institute KITANO HOSPITAL, PIIF Tazuke-kofukai, Kita-ku, Osaka 530-8480, Japan
[6]Lead contact
*Correspondence: ichiroy@kuhp.kyoto-u.ac.jp
https://doi.org/10.1016/j.isci.2024.111565

SUMMARY

Activation of thyroid-stimulating hormone receptor (TSHR) fundamentally leads to hyperthyroidism. To elucidate TSHR signaling, we conducted transcriptome analyses for hyperthyroid mice that we generated by overexpressing TSH. TSH overexpression drastically changed their thyroid transcriptome. In particular, enrichment analyses identified the cell cycle, phosphatidylinositol 3-kinase/Akt pathway, and Ras-related protein 1 pathway as possibly associated with goiter development. Regarding hyperthyroidism, *Slc26a4* was exclusively upregulated with TSH overexpression among genes crucial to thyroid hormone secretion. To verify its significance, we overexpressed TSH in *Slc26a4* knockout mice. TSH overexpression caused hyperthyroidism in *Slc26a4* knockout mice, equivalent to that in control mice. Thus, we did not observe significant changes in known genes and pathways involved in thyroid hormone secretion with TSH overexpression. Our datasets might include candidate genes that have not yet been identified as regulators of thyroid function. Our transcriptome datasets regarding hyperthyroidism can contribute to future research on TSHR signaling.

INTRODUCTION

Hyperthyroidism is a condition in which excessive secretion of thyroid hormones elevates their circulating levels, leading to various symptoms and metabolic abnormalities. Graves' disease is the most common cause of hyperthyroidism; its incidence is as high as 20–40 cases per 100,000 population.[1] First-line therapy of Graves' disease has been conservative in the past several decades: anti-thyroid drugs (ATDs) that inhibit thyroid hormone secretion and radioactive iodine therapy. Physicians in Europe, Latin America, and Japan prefer ATDs.[2] Increased use of ATDs and decreased use of radioactive iodine therapy were recently observed in the United States.[3]

ATDs are used by many patients, and they have various adverse effects. Among major ATDs, thiamazole (MMI) and propylthiouracil (PTU) often cause liver injury and rash. They can cause agranulocytosis that progresses into life-threating infections. Furthermore, MMI should be avoided during the first trimester of pregnancy due to teratogenicity.[4,5] PTU use is not recommended for children as first-line therapy due to the high incidence of severe liver injury and vasculitis.[6] Treatment of hyperthyroidism can sometimes be challenging because of these problems and insufficient effects with conventional ATDs. However, there are few promising candidates for new ATDs that inhibit thyroid hormone secretion.

The pathophysiology of hyperthyroidism can provide conceptions of new ATDs. Hyperthyroidism fundamentally develops as a result of thyroid-stimulating hormone receptor (TSHR) stimulation in the thyroid gland. Autoantibodies stimulate TSHRs in Graves' disease.[1] Toxic adenoma, a thyroid neoplasm with the autonomous secretion of thyroid hormones, is another cause of hyperthyroidism. It is often associated with somatic mutations in the *TSHR* gene that result in its constitutive activation.[7–10] TSHR is a G protein-coupled receptor that primarily couples to G proteins that activate the protein kinase A (PKA) pathway through increasing cyclic adenosine monophosphate (cAMP) production.[11] In addition, TSHR can couple to Gq/11 and activate the phospholipase C cascade with a high concentration of TSH ligands.[12,13] As a result of such downstream pathways, TSHR activation increases thyroid hormone secretion and enlarges the thyroid gland, as usually seen in patients with Graves' disease.

Although the outlines of TSHR signaling are known, detailed mechanisms at the molecular level remain to be elucidated. Previous studies have identified thyroglobulin (TG), thyroid peroxidase (TPO), sodium iodide symporter (SLC5A5), type 2

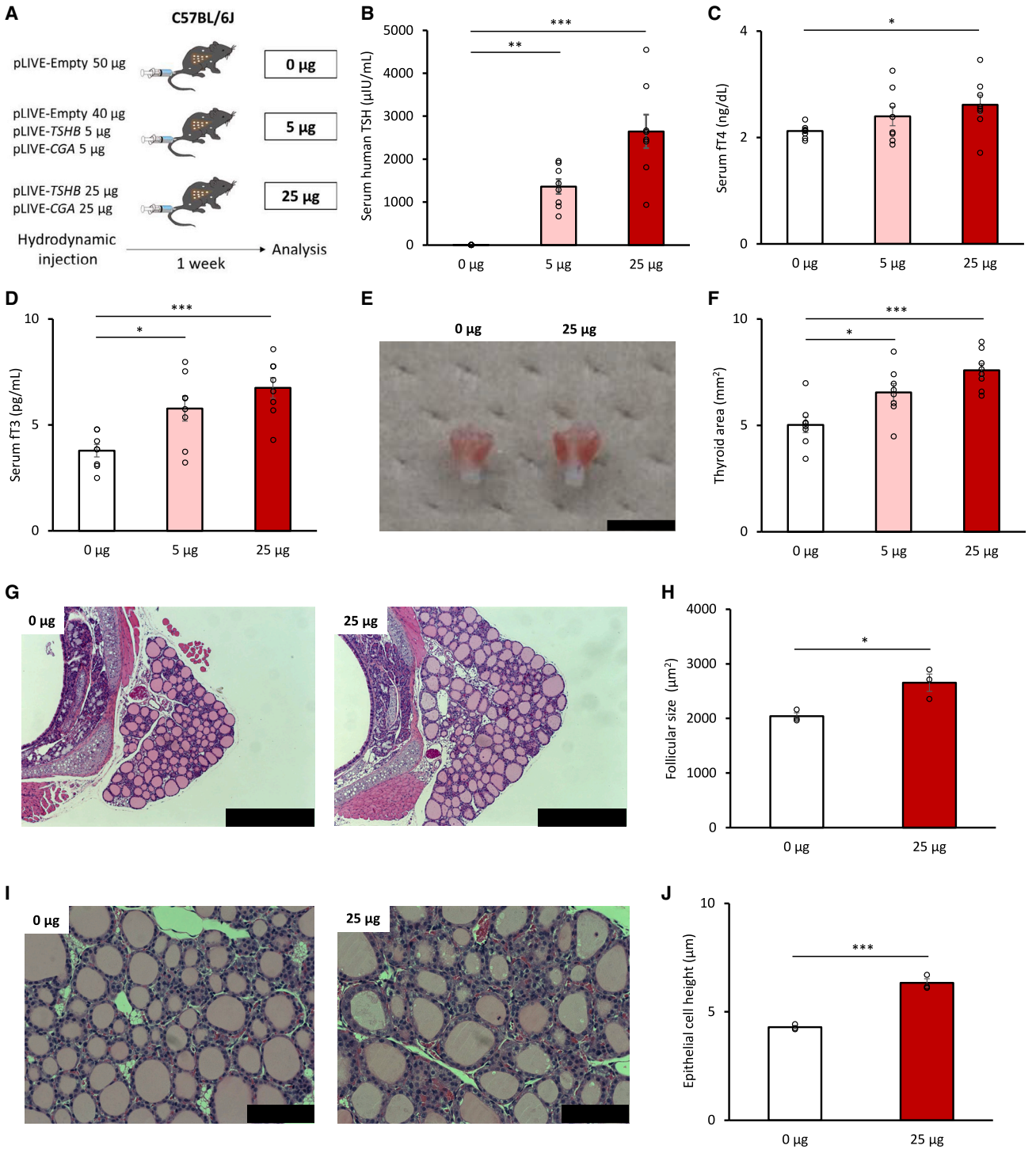

Figure 1. Phenotypes of mice overexpressing thyroid-stimulating hormone (TSH) at 1 week after hydrodynamic gene delivery

(A) Schema for the experimental design by dose of vectors injected. *n* = 8 for each group.

(B–D) Serum levels of thyroid hormones. fT4, free thyroxine; fT3, free triiodothyronine.

(E) Gross appearance of thyroid glands. The black scale bar is 5 mm.

(F) Thyroid gland size measured as thyroid area based on photographs.

(G) Histological images of thyroid glands with hematoxylin and eosin staining at 50× magnification. The black scale bar is 500 μm.

(H) Mean follicle size is calculated based on histological images. *n* = 3 each.

(legend continued on next page)

iodothyronine deiodinase, and TSHR as molecules affected by TSHR activation.[14–17] Except for TG, these results were verified via experiments involving *in vitro* TSH administration, whereas thyroid hormone synthesis progresses in thyroid follicles consisting of follicular epithelial cells *in vivo*. It is likely that iodine concentrations in thyroid follicles are varied in hyperthyroidism because TSH increases thyroidal levels of SLC5A5, the main transporter of iodine into the thyroid gland.[18] Iodine is a regulator of thyroid hormone secretion itself, which is known as the Wolff-Chaikoff effect; iodine administration represses thyroid hormone secretion with the attenuation of thyroidal SLC5A5 expression.[19] In this context, we believe that *in vivo* experiments to analyze cells maintaining follicular structure are necessary.

In the present study, we conducted *in vivo* experiments to understand the molecular landscape of background TSHR signaling in hyperthyroidism. Previous studies of *in vitro* TSH administration had limitations because they did not consider changes in the condition of thyroid follicles. To date, *in vivo* models of hyperthyroidism have been generated by the immunization of TSHR protein to replicate Graves' disease,[20] but the immunized animals do not consistently develop hyperthyroidism, even in recent models.[21] Furthermore, the strategy of immunization might cause bias due to the lymphocyte infiltration of the thyroid gland. We believe that hyperthyroid animals without immunization are more suitable for studying hyperthyroidism. Here, we demonstrate the phenotypes of our hyperthyroid mice generated by TSH overexpression using *in vivo* transfection and transcriptome datasets of their thyroid glands.

RESULTS

Generation of hyperthyroid mice

We generated mice with hyperthyroidism through the continuous activation of TSHR achieved by providing excessive concentrations of its ligand, TSH. To accomplish this strategy, we developed a method for overexpressing TSH via *in vivo* transfection with hydrodynamic gene delivery.[22] TSH forms a heterodimer consisting of a specific β subunit encoded by *TSHB*[23] and an α subunit coded by *CGA* that is common to luteinizing hormone, follicle-stimulating hormone, and chorionic gonadotropin.[24] Therefore, we cloned human *TSHB* and *CGA* genes into pLIVE vectors and hydrodynamically injected 25 μg of these vectors into C57BL/6J mice according to our previous studies.[25–27] At 1 week after hydrodynamic gene delivery, human TSH was not detected in the serum when each vector was separately injected, but TSH was strongly detected when both vectors were co-injected (Figure S1A). Furthermore, we observed elevated concentrations of serum free thyroxine (fT4) and free triiodothyronine (fT3) in co-injected mice (Figures S1B and S1C).

Thereafter, the effects of TSH overexpression based on transfection with both pLIVE-*TSHB* and pLIVE-*CGA* vectors were further verified at 1 week after hydrodynamic gene delivery. We determined the dose-dependent effects by analyzing 3 groups based on the amount of injected vectors (Figure 1A). Human TSH was detected in the serum of the 5 μg group and at higher levels in the 25 μg group (Figure 1B). pLIVE-Empty vector was injected with pLIVE-*TSHB* and pLIVE-*CGA* vectors in the 0 μg and 5 μg groups to ensure the total amount of injected vectors was 50 μg (Figure 1A). Dose-dependent increases were also observed in serum levels of fT4 and fT3 (Figures 1C and 1D), which was further verified by their positive correlations with serum human TSH levels: fT4 and TSH, $r = 0.74$ ($p < 0.001$) and fT3 and TSH, $r = 0.77$ ($p < 0.001$) (Figures S1D and S1E).

In addition to these expected changes in the serum, we found enlargement of the thyroid gland after transfection (Figure 1E). Goiters developed in a dose-dependent manner (Figure 1F); goiter severity was positively correlated with serum human TSH levels ($r = 0.53$, $p < 0.05$) (Figure S1F). Histological changes in the thyroid gland included increases in follicle size (Figures 1G and 1H) and follicular epithelial cell height (Figures 1I and 1J). With TSH overexpression, lymphocytic infiltration was not apparent (Figure 1G), whereas colloids with peripheral scalloping, which is a feature of hyperthyroidism, appeared in some follicles (Figure 1I).

Recent evidence has shown that thyroid hormones are influenced by the circadian rhythm.[28–30] We analyzed mice at the end of both the dark and light cycles. In mice without TSH overexpression, serum fT3 levels were higher at the end of the dark cycle, consistent with previous studies,[28,29] while serum fT4 levels and pituitary *Tshb* mRNA did not show significant changes (Figure S2). In mice overexpressing TSH, the levels of overexpressed human TSH, as well as serum levels of fT4 and fT3, did not differ significantly between the end of the light cycle and the dark cycle (Figures S2A–S2C). In addition, pituitary *Tshb* mRNA was markedly decreased due to TSH overexpression at both the end of the light and dark cycles (Figures S2D and S2E).

Subsequently, we evaluated the persistence of induced hyperthyroidism by analyzing mice at 4 weeks after hydrodynamic gene delivery (Figure 2A). Human TSH was still detected in a dose-dependent manner (Figure 2B). Accordingly, increases in serum levels of fT4 and fT3 persisted (Figures 2C and 2D). Goiter development was also seen in a dose-dependent manner (Figures 2E and 2F). Serum human TSH levels were positively correlated with serum levels of fT4 and fT3 (fT4 and TSH, $r = 0.81$ ($p < 0.001$); fT3 and TSH, $r = 0.65$ ($p < 0.001$) and with goiter severity (thyroid area and TSH, $r = 0.78$ ($p < 0.001$)) (Figures S1G–S1I). Histological changes after 4 weeks were partially inconsistent with those after 1 week. Follicle size was similarly increased (Figures 2G and 2H), but follicular epithelial cell height was decreased (Figures 2I and 2J). Lymphocytic infiltration was not observed (Figure 2G), and unlike after 1 week, colloids with peripheral scalloping were not found in any follicles (Figure 2I). During TSH overexpression for 4 weeks, the body weight of

(I) Histological images of thyroid glands with hematoxylin and eosin staining at 200× magnification. The black scale bar is 100 μm.

(J) Epithelial cell height is measured based on histological images. $n = 3$ each. Data are represented as means ± standard error of the mean (SEM). Statistical analyses were performed using one-way analysis of variance (ANOVA) followed by the Dunnett test with comparison to the 0 μg group for panels B–D and F and using Student's *t*-test for panels H and J. $^{*}p < 0.05$, $^{**}p < 0.01$, and $^{***}p < 0.001$.

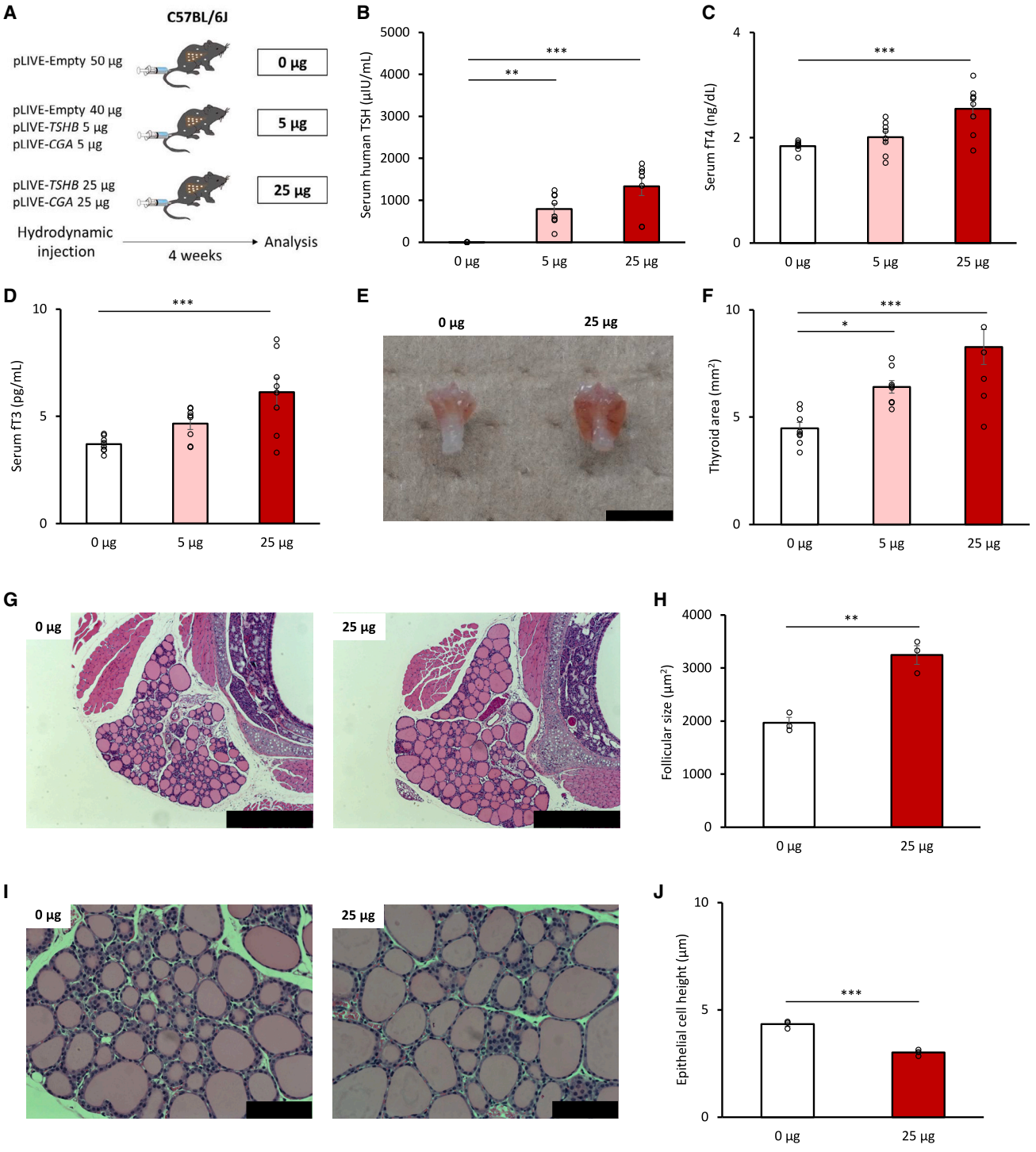

Figure 2. Phenotypes of mice overexpressing TSH at 4 weeks after hydrodynamic gene delivery

(A) Schema for the experimental design by dose of vectors injected. *n* = 8 for each group.

(B–D) Serum levels of thyroid hormones.

(E) Gross appearance of thyroid glands. The black scale bar is 5 mm.

(F) Thyroid gland size measured as thyroid area based on photographs.

(G) Histological images of thyroid glands with hematoxylin and eosin staining at 50× magnification. The black scale bar is 500 μm.

(H) Mean follicle size is calculated based on histological images. *n* = 3 each.

(legend continued on next page)

hyperthyroid mice gradually increased (Figures S3A and S3B). In addition, they consumed more water and food (Figures S3C–S3F).

Thyroid transcriptome of hyperthyroid mice

Our hyperthyroid mice exhibited excessive secretion of thyroid hormones and goiter development through the effects of TSH overexpression. Using this model, we subsequently obtained data on the thyroid transcriptome using RNA sequencing (RNA-seq). In addition to investigating TSHR signaling, we aimed to clarify mechanisms of ATD action to obtain therapeutic targets for hyperthyroidism. We designed the experiment as follows (Figure 3A): the TSH group was injected with 25 μg each of the pLIVE-*TSHB* and pLIVE-*CGA* vectors and the Empty group was injected with 50 μg of the pLIVE-Empty vector. The mice were further treated with MMI in their drinking water and analyzed after 1 week.

Hyperthyroidism was reproducibly achieved in the TSH group, which was seen as an increase in serum levels of fT4 and fT3 (Figures 3B and S4A). We could match serum fT4 levels of the TSH-MMI group with those of the Empty group to avoid biases arising from differences in circulating levels of thyroid hormones (Figure 3B). TSH was equivalently detected in the serum of the TSH and TSH-MMI groups (Figure 3C). MMI administration in the presence of TSH overexpression shrank goiter (Figures S4B and S4C) and decreased follicle size (Figures S4D and S4E), but did not change follicular epithelial cell height (Figures S4F and S4G).

The RNA-seq dataset of their thyroid glands is presented in Table S1. Clustering and principal component analyses revealed clear differences between the Empty and TSH groups, whereas slight differences were observed between the TSH and TSH-MMI groups (Figures 3D and 3E). As for differentially expressed genes (DEGs), TSH overexpression substantially upregulated 701 genes and downregulated 473 genes, while MMI administration in the presence of TSH overexpression only upregulated 34 genes and downregulated 43 genes (Figures 3F–3H).

In addition, similar analyses were performed at 4 weeks after hydrodynamic gene delivery (Figure 4A). MMI was only administered during the last week. Induction of hyperthyroidism was verified; the TSH group had increased serum levels of fT4 and fT3 (Figures 4B and S5A). Similarly to the result at 1 week, MMI administration decreased serum fT4 levels in the TSH-MMI group equivalent to those of the Empty group (Figure 4B). TSH overexpression was confirmed based on elevated serum human TSH levels (Figure 4C). MMI administration did not attenuate increases in thyroid gland size, follicle size, or follicular epithelial cell height caused by TSH overexpression (Figures S5B–S5G).

At 4 weeks, we performed RNA-seq for all 4 groups (Table S2). Clustering and principal component analyses revealed differences between the Empty and TSH groups as well as between the Empty and Empty-MMI groups, whereas no clear differences were seen between the TSH and TSH-MMI groups (Figures 4D and 4E). In terms of DEGs, TSH overexpression substantially upregulated 497 genes and downregulated 435 genes, while MMI administration in the presence of overexpressed TSH only upregulated 43 genes and downregulated 66 genes (Figures 4F–4H). On the other hand, MMI administration without TSH overexpression upregulated 143 genes and downregulated 236 genes (Figures S6A and S6B). We picked 17 genes crucial to thyroid hormone secretion, referred to as thyroidal genes, and examined their changes. MMI administration in the presence and absence of TSH overexpression altered a few thyroidal genes (Figures S6C–S6E).

Moreover, we treated hyperthyroid mice with PTU and analyzed them 1 week after hydrodynamic gene delivery (Figure S7). PTU administration did not change serum fT3 levels but decreased serum fT4 levels (Figures S7A and S7B). TSH was equivalently detected in the serum of the TSH and TSH-PTU groups (Figure S7C). No significant changes were observed in selected thyroidal genes examined by quantitative RT-PCR (Figures S7D and S7E). Since serum fT3 levels were not decreased by either MMI or PTU administration, we administered a 10-fold higher concentration of either MMI (TSH-MMI high) or PTU (TSH-PTU high) to verify their anti-thyroid effects. Although overexpressed TSH levels were higher in the TSH-MMI high and TSH-PTU high groups compared to the TSH group (Figure S8A), serum fT4 levels decreased in the TSH-MMI high and TSH-PTU high groups (Figure S8B). In addition, serum fT3 levels decreased in the TSH-PTU high group (Figure S8C).

As we have found small changes in the thyroid transcriptome with the administration of ATDs, we focused on comparisons between the TSH and Empty groups in the following analyses. Enrichment analyses were performed using gene ontology (GO) and the Kyoto Encyclopedia of Genes and Genomes (KEGG). We compared the TSH group with the Empty group. Results at 1 week are shown in Figure 5 and those at 4 weeks are in Figure 6. At 1 week, terms related to the cell cycle were often seen with TSH overexpression (Figure 5). Results of MMI administration without TSH overexpression at 4 weeks are shown in Figure S9. Through these analyses, we could not find remarkable terms related to hyperthyroidism.

We examined individual DEGs and listed the top 30 genes upregulated with TSH overexpression. At 1 week, we found upregulated genes associated with the cell cycle such as *Cdkn3*, *Plk1*, and *Ccnb1*, which was consistent with the results of enrichment analyses (Table 1). In addition, we found *Dio3* upregulation at 4 weeks (Table 2) and checked all 3 iodothyronine deiodinases. RNA-seq results showed that *Dio1*, *Dio2*, and *Dio3* were upregulated at 1 week, and *Dio2* and *Dio3* were upregulated at 4 weeks (Figures S10A and S10B). Using quantitative RT-PCR analyses, we determined *Dio2* upregulation with TSH overexpression at 4 weeks (Figures S10C–S10F). A detailed search of our RNA-seq datasets highlighted antioxidant responses. A GO term "antioxidant activity" was enriched with TSH overexpression ($p = 0.026$ at 1 week) (Table S3). We

(I) Histological images of thyroid glands with hematoxylin and eosin staining at 200× magnification. The black scale bar is 100 μm.

(J) Epithelial cell height is measured on histological images. $n = 3$ each. Data are represented as means ± SEM. Statistical analyses were performed using ANOVA followed by the Dunnett test with comparison to the 0 μg group for panels B–D and F and using Student's *t*-test for panels H and J. $^{*}p < 0.05$, $^{**}p < 0.01$, and $^{***}p < 0.001$.

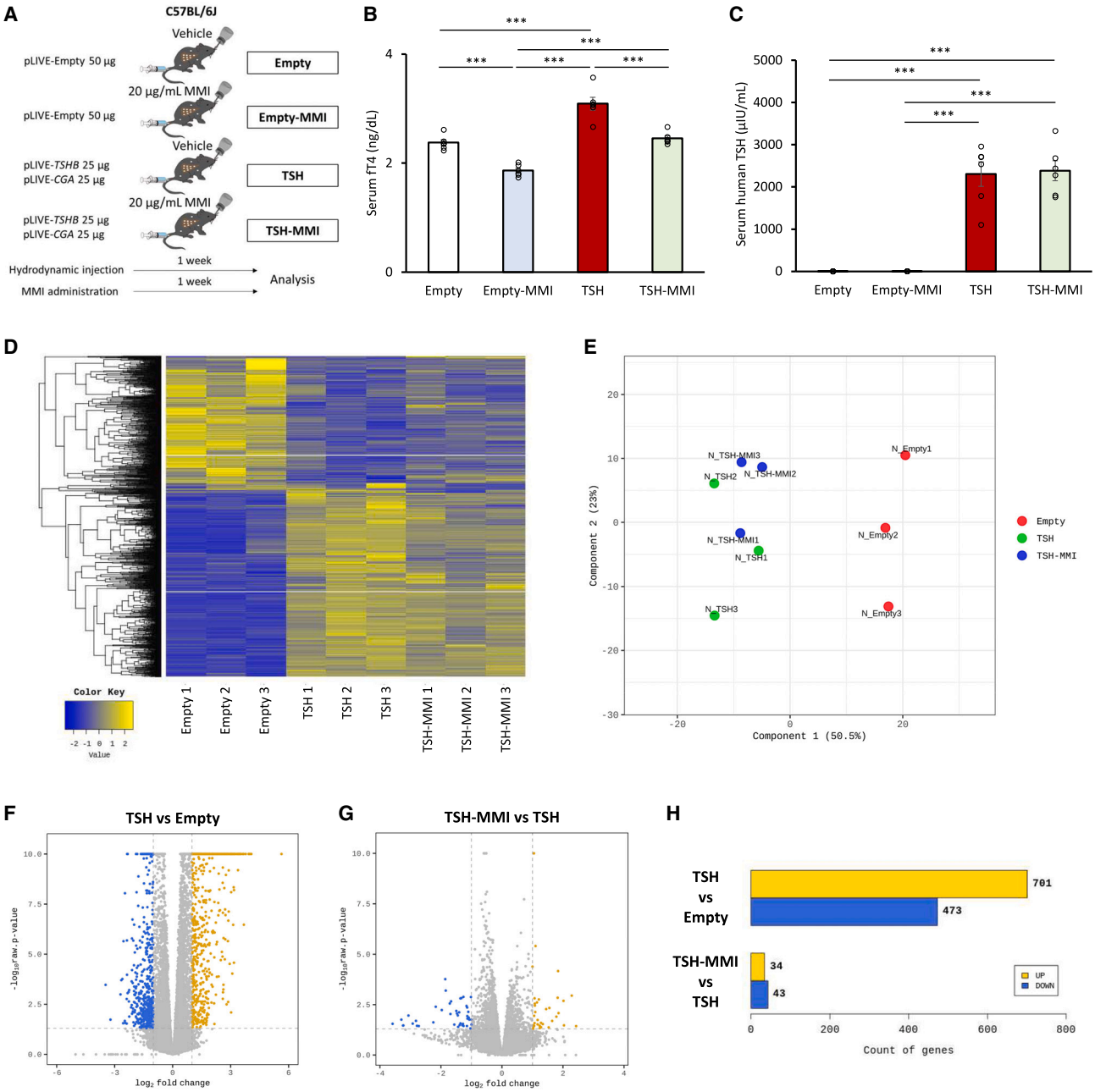

Figure 3. Transcriptome analyses of the thyroid glands of mice overexpressing TSH at 1 week after hydrodynamic gene delivery

(A) Schema for the experimental design. Thiamazole (MMI) was continuously administered via drinking water at 20 μg/mL.

(B and C) Serum levels of thyroid hormones. $n = 6$ each. (D–H) Summary of results of RNA sequencing (RNA-seq). $n = 3$ each, selected based on the proximity of serum fT4 levels to the average of each group.

(D) Hierarchical clustering, (E) principal component analysis, (F) volcano plot of differentially expressed genes (DEGs) comparing the TSH and Empty groups, (G) volcano plot of DEGs comparing the TSH-MMI and TSH groups, and (H) numbers of DEGs in each comparison. Data are represented as means ± SEM. Statistical analyses were performed using ANOVA followed by the Tukey-Kramer test. ***$p < 0.001$.

selected antioxidant genes, *Gpx2*, *Sod3*, *Srxn1*, *Txnrd1*, *Upk3bl*, and *Nqo1*, from this GO term and previous reports.[31] In the RNA-seq results, these 6 genes were all upregulated with TSH overexpression at both 1 week and 4 weeks (Figures S11A and S12A). Through quantitative RT-PCR analyses, we confirmed that TSH overexpression upregulated *Srxn1* at 1 week (Figures S11B and S11C) and *Srxn1*, *Txnrd1*, and *Upk3bl* at 4 weeks (Figures S12B and S12C).

It was noteworthy that *Slc26a4* had the second highest change at 1 week (Table 1). Upregulation of *Slc26a4* was

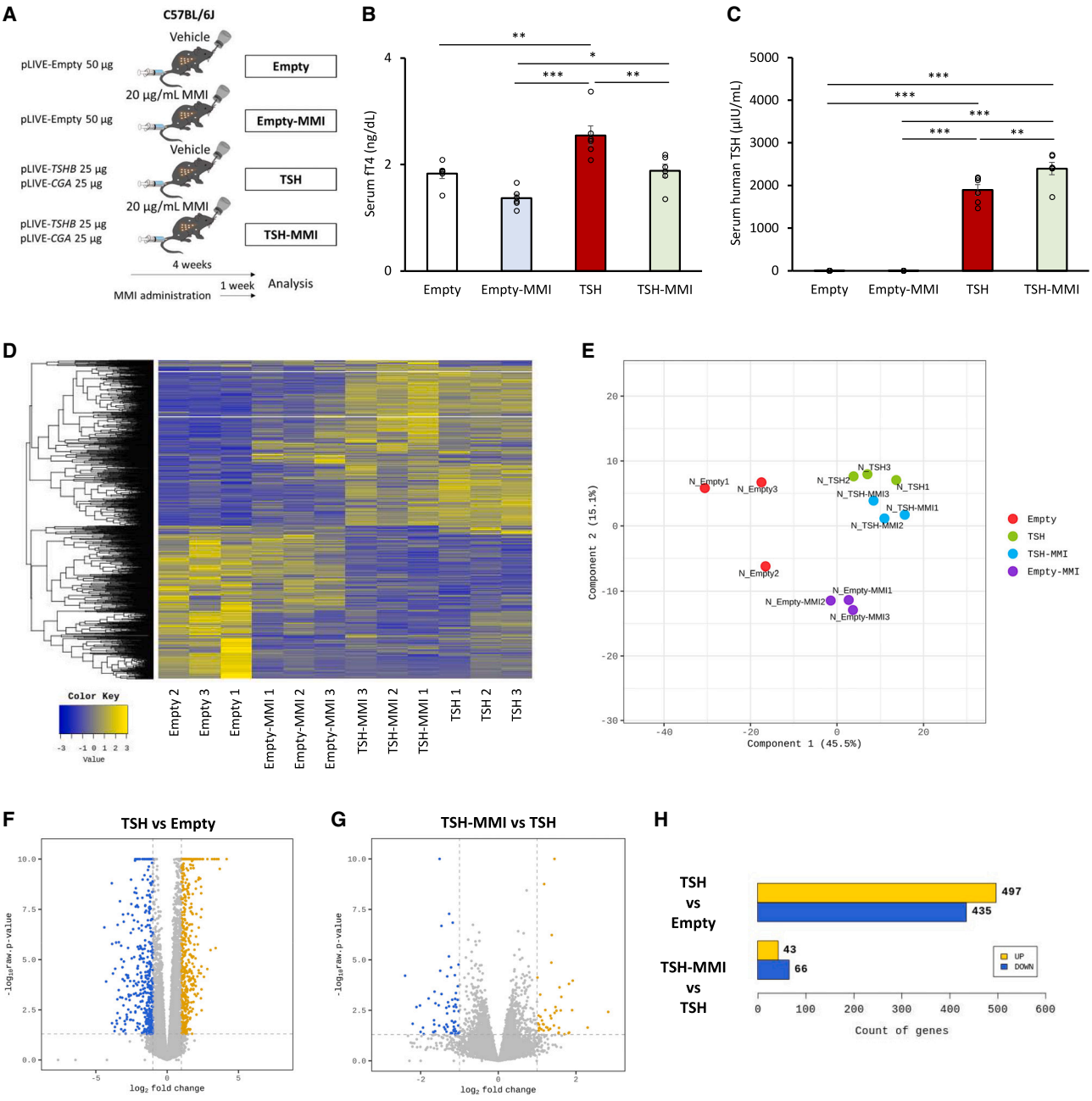

Figure 4. Transcriptome analyses of the thyroid glands of mice overexpressing TSH at 4 weeks after hydrodynamic gene delivery

(A) Schema for the experimental design. MMI was administered only for the last week.

(B and C) Serum levels of thyroid hormones. $n = 6$ each.

(D–H) Summary of results of RNA-seq. $n = 3$ each, selected based on the proximity of serum fT4 levels to the average of each group. (D) Hierarchical clustering, (E) principal component analysis, (F) volcano plot of DEGs comparing the TSH and Empty groups, (G) volcano plot of DEGs comparing the TSH-MMI and TSH groups, and (H) numbers of DEGs in each comparison. Data are represented as means ± SEM. Statistical analyses were performed using ANOVA followed by the Tukey-Kramer test. $^{*}p < 0.05$, $^{**}p < 0.01$, and $^{***}p < 0.001$.

similarly observed at 4 weeks (Table 2). We reviewed the datasets for thyroidal genes, which revealed that *Slc26a4* was exclusively upregulated at both 1 and 4 weeks (Figure 7). However, it was surprising that other iodine transporters, particularly *Slc5a5*, were not altered. We wondered whether SLC5A5 transiently increased and then attenuated, as an increase in *SLC5A5* mRNA at 24 h after TSH administration disappeared at 48 h in the previous study using human thyrocytes.[17] Therefore, we analyzed the mice 1 day after hydrodynamic gene delivery. Hyperthyroidism had already developed, as evidenced by

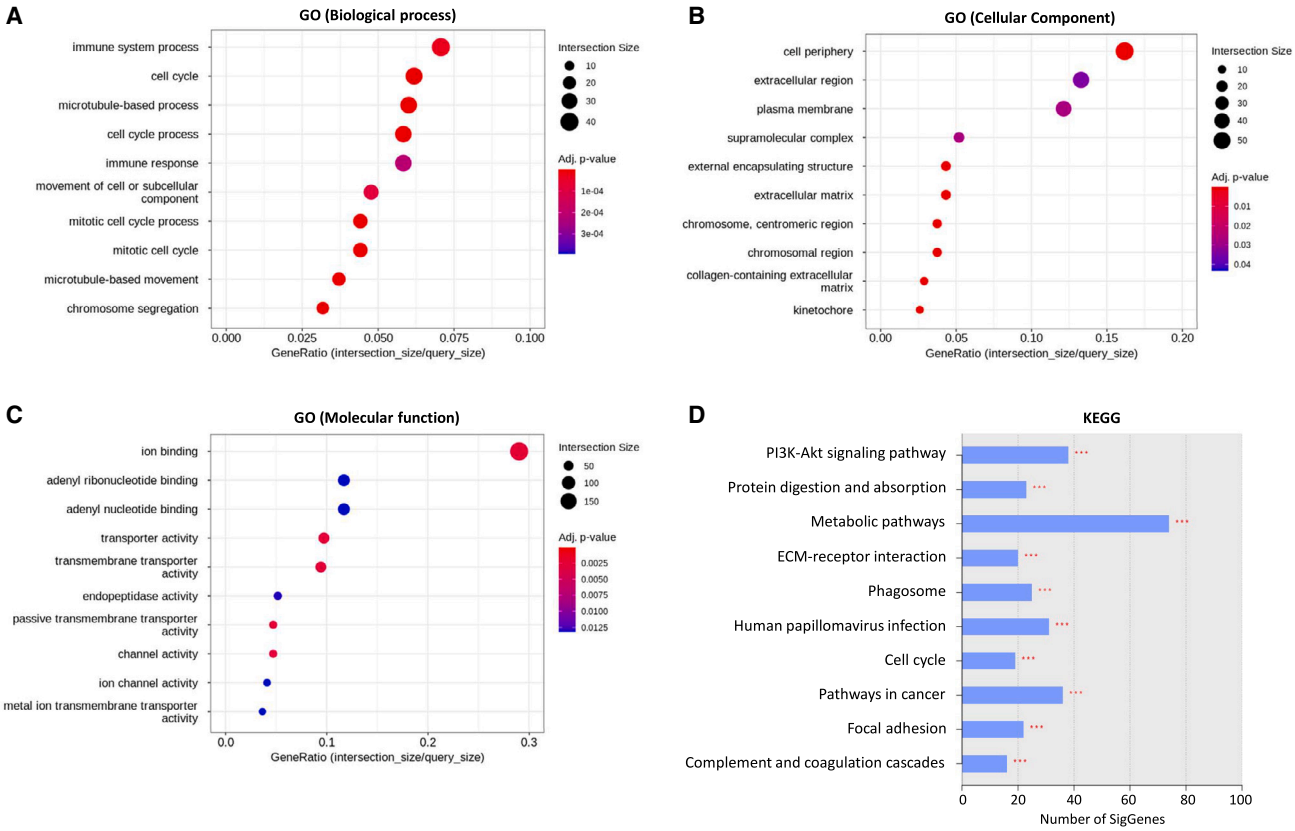

Figure 5. Top 10 terms in enrichment analyses of the TSH group compared with the Empty group at 1 week after hydrodynamic gene delivery

(A–C) Gene Ontology (GO) terms.

(D) Kyoto Encyclopedia of Genes and Genomes (KEGG) terms. Statistical analyses were performed using Fisher's exact test. $^{*}p < 0.05$, $^{**}p < 0.01$, and $^{***}p < 0.001$.

increased serum levels of TSH, fT4, and fT3 (Figures S13A–S13C). Thyroid lysates of mice overexpressing TSH had higher levels of cAMP, T4, and T3, suggesting overproduction of thyroid hormones through TSHR stimulation (Figures S13D–S13F). Quantitative RT-PCR analyses revealed that mRNAs of *Slc5a5* as well as *Tshr* and *Tpo* increased at 1 day (Figures S14A and S14B) and that these increases were not observed after 1 week (Figures S14C and S14D). *Tg* mRNA decreased at both 1 day and 1 week, whereas *Slc26a4* mRNA increased only from 1 week after hydrodynamic gene delivery (Figure S14).

Thyroid-stimulating hormone overexpression in Slc26a4 knockout mice

Slc26a4, an exclusive thyroidal gene upregulated in our hyperthyroid mice, codes the SLC26A4 protein, also known as pendrin. SLC26A4 is an apical iodine transporter that transports iodine into thyroid follicles, which is important for thyroid hormone secretion. Attenuation of SLC26A4 action can cause hypothyroidism. Loss-of-function mutations in *SLC26A4* are known to cause Pendred syndrome, which includes hypothyroidism.[32] However, it remains unclear whether SLC26A4 upregulation contributes to hyperthyroidism. We wondered whether hyperthyroidism becomes milder when *Slc26a4* is not upregulated in response to TSH overexpression.

Therefore, we analyzed *Slc26a4* knockout mice. More specifically, we caused hyperthyroidism via TSH overexpression in heterozygous (Hetero-TSH group) and homozygous *Slc26a4* knockout mice (Homo-TSH group). We compared them with mice injected with pLIVE-Empty vector (Hetero-Empty and Homo-Empty groups) (Figure 8A). The concentration of vectors injected was doubled because *Slc26a4* knockout mice somehow exhibited relatively low serum levels of human TSH with TSH overexpression (Figure 8B). Nevertheless, the Hetero-TSH and Homo-TSH groups certainly developed hyperthyroidism and goiters (Figures 8C–8F). No significant differences in serum levels of fT4, fT3, or human TSH were observed between the Hetero-TSH and Homo-TSH groups (Figures 8B–8D). Goiter severity was also similar between the Hetero-TSH and Homo-TSH groups (Figures 8E and 8F). Although follicle size and follicular epithelial cell height were significantly increased with TSH overexpression, no differences were observed between the Hetero-TSH and Homo-TSH groups (Figures 8G–8J).

We carefully verified these results through the following examinations. In heterozygous *Slc26a4* knockout mice, there was a significant increase in *Slc26a4* mRNA levels in the thyroid gland with TSH overexpression (Figures S15A and S15B). Examination of selected thyroidal genes revealed lower mRNA levels of *Tg*, *Tpo*, and *Slc5a5* with TSH overexpression in heterozygous

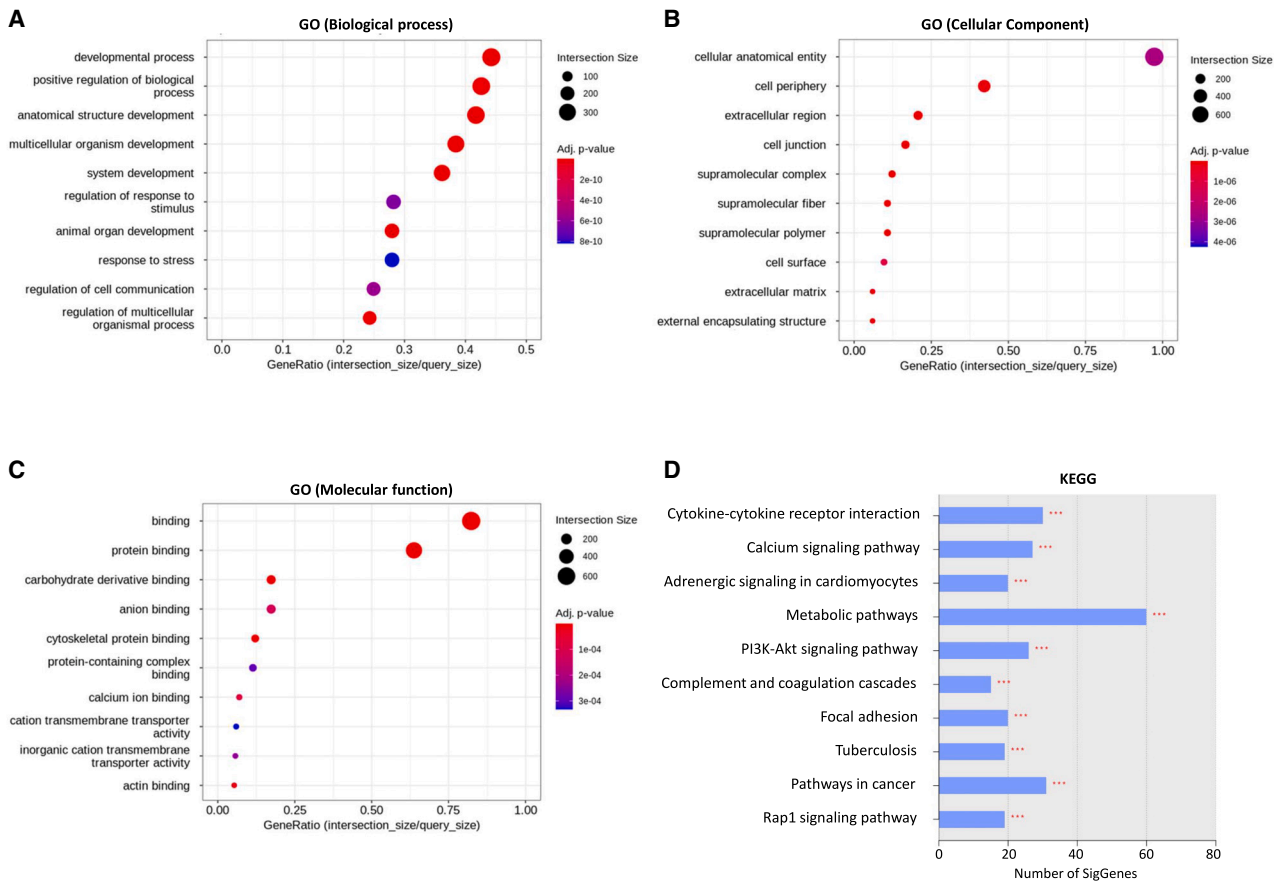

Figure 6. Top 10 terms in enrichment analyses of the TSH group compared with the Empty group at 4 weeks after hydrodynamic gene delivery

(A–C) GO terms.

(D) KEGG terms. Statistical analyses were performed using Fisher's exact test. ***$p < 0.001$.

Slc26a4 knockout mice, while no significant changes were observed in homozygous *Slc26a4* knockout mice (Figures S15C and S15D). This result raised a concern that the downregulation of *Tg*, *Tpo*, and *Slc5a5* attenuates hyperthyroidism induction in heterozygous *Slc26a4* knockout mice, regardless of SLC26A4 levels.

To address this concern and confirm reproducibility, we performed additional analyses 3 days after hydrodynamic gene delivery (Figure S16A). Both heterozygous and homozygous *Slc26a4* knockout mice had increases in serum human TSH levels with TSH overexpression (Figure S16B) and developed equivalent degrees of hyperthyroidism as determined based on serum fT4 levels (Figure S16C). Serum fT3 levels were also significantly increased in heterozygous *Slc26a4* knockout mice and insignificantly increased in homozygous *Slc26a4* knockout mice (Figure S16D). Increases in *Slc26a4* mRNA levels with TSH overexpression in heterozygous *Slc26a4* knockout mice were also confirmed (Figures S16E and S16F). Homozygous *Slc26a4* knockout mice did not have *Slc26a4* mRNA (Figure S16G). However, the SLC26A4 protein was difficult to detect in the thyroid glands of heterozygous *Slc26a4* knockout mice (Figure S16H). We could not detect SLC26A4 protein in the thyroid glands of heterozygous *Slc26a4* knockout mice with TSH overexpression, even though *Slc26a4* mRNA levels were increased (Figure S16I). These results suggested that the SLC26A4 protein is slightly or not expressed in the murine thyroid gland. Examination of selected thyroidal genes revealed decreases in levels of *Tg* and *Slc5a5* mRNA with TSH overexpression in both heterozygous and homozygous *Slc26a4* knockout mice, while other genes were not changed (Figure S17).

DISCUSSION

In the present study, we generated hyperthyroid mice through TSH overexpression with hydrodynamic gene delivery using both pLIVE-*TSHB* and pLIVE-*CGA* vectors. The hyperthyroid mice consistently developed hyperthyroidism and goiters for at least 4 weeks. We conducted transcriptome analysis on their thyroid glands to elucidate TSHR signaling. Although few changes in the thyroid transcriptome were observed when the hyperthyroid mice were treated with MMI, drastic changes were induced with TSH overexpression at both 1 and 4 weeks

Table 1. Top 30 upregulated genes with TSH overexpression at 1 week

Gene symbol	Description	Fold change	*p*
Slc34a2	solute carrier family 34 (sodium phosphate), member 2	49.629	4.565E-16
Slc26a4	solute carrier family 26, member 4	16.791	3.792E-32
Cpn1	carboxypeptidase N, polypeptide 1	15.877	3.504E-16
Iqgap3	IQ motif containing GTPase-activating protein 3	15.262	3.477E-112
Pimreg	PICALM interacting mitotic regulator	13.744	3.119E-48
Car15	carbonic anhydrase 15	12.854	3.378E-07
Ckap2	cytoskeleton associated protein 2	12.757	5.599E-50
Hmmr	hyaluronan mediated motility receptor (RHAMM)	12.367	1.693E-71
Depdc1a	DEP domain containing 1a	11.584	3.285E-20
Kif20a	kinesin family member 20A	11.492	8.039E-81
Cdkn3	cyclin-dependent kinase inhibitor 3	11.337	2.997E-26
Prc1	protein regulator of cytokinesis 1	11.208	4.640E-65
Bcat1	branched chain aminotransferase 1, cytosolic	11.131	1.822E-22
Plk1	Polo-like kinase 1	10.856	4.702E-12
Cenpf	centromere protein F	10.772	2.817E-14
Gdf15	growth differentiation factor 15	10.744	2.149E-19
Cep55	centrosomal protein 55	10.562	1.001E-28
Kif18b	kinesin family member 18B	10.473	4.677E-26
C330021F23Rik	RIKEN cDNA C330021F23 gene	10.422	6.420E-10
Col11a2	collagen, type XI, alpha 2	10.141	1.688E-22
Ccn5	cellular communication network factor 5	9.972	1.156E-38
Knstrn	kinetochore-localized astrin/SPAG5 binding	9.445	1.575E-40
Erfe	erythroferrone	9.266	1.034E-18
Kif2c	kinesin family member 2C	9.208	8.449E-28
Ube2c	ubiquitin-conjugating enzyme E2C	9.030	6.304E-09
Aspm	abnormal spindle microtubule assembly	9.000	5.567E-36
Ccnb1	cyclin B1	8.937	4.578E-09
Anln	anillin, actin binding protein	8.899	9.955E-67
Rph3a	rabphilin 3A	8.861	1.257E-13
Pbk	PDZ binding kinase	8.820	1.939E-39

TSH, thyroid stimulating hormone. Fold changes between the TSH and Empty group in transcripts per kilobase million (TPM) of genes are represented. Statistical analyses were performed with the Wald test.

after hydrodynamic gene delivery. We found that *Slc26a4* is the only upregulated thyroidal gene at both 1 and 4 weeks. To examine whether SLC26A4 is associated with the development of hyperthyroidism, we caused hyperthyroidism in *Slc26a4* knockout mice. *Slc26a4* knockout mice certainly developed hyperthyroidism through TSH overexpression, but had similar degrees of hyperthyroidism as control mice.

Several murine models of hyperthyroidism have been generated through immunization with TSHR protein.[20,21] Interestingly, Jaeschke et al. generated mice with a knocked-in human *TSHR* sequence that had a constitutively active mutation.[33] Serum fT4 levels were higher in the homozygous *TSHR* knock-in mice. Goiters developed in both the heterozygous and homozygous *TSHR* knock-in mice. Hyperthyroidism developed at 1 month of age while goiters developed at 2 months of age. Our hyperthyroid mice and *TSHR* knock-in mice were similar in that both had TSHR activation and developed hyperthyroidism with goiters. Hyperthyroidism in our hyperthyroid mice was guaranteed with histologic changes such as colloids with peripheral scalloping and increased thyroidal T4 and T3. Although *in vitro* studies suggested that TSHR activation can alter *TPO*, *SLC5A5*, *TSHR*, and so on,[14–17] TSH overexpression did not alter the expression of these genes in our *in vivo* system at either 1 week or 4 weeks. Considering that mRNAs of *Tpo*, *Slc5a5*, and *Tshr* increased at 1 day after hydrodynamic gene delivery, feedback reactions occurring in follicles might contribute to the interruption of the changes observed at 1 day.

Although the increases in serum fT4 and fT3 levels were not pronounced in our hyperthyroid mice, the observed decreases in pituitary *Tshb* mRNA, along with increased food and water consumption, confirmed a significant hyperthyroid state. In our previous study, which administered 3,3′,5-triiodo-L-thyronine (LT3) via drinking water to hypothyroid mice, pituitary *Tshb* mRNA decreased with the administration of 0.1 μg/mL of LT3, leading to the upregulation of thyroid hormone responsive gene expressions in several organs.[34] Our hyperthyroid mice

Table 2. Top 30 upregulated genes with TSH overexpression at 4 weeks

Gene symbol	Description	Fold change	*p*
Slc34a2	solute carrier family 34 (sodium phosphate), member 2	18.009	2.176E-22
Oas1d	2′-5′ oligoadenylate synthetase 1D	12.893	3.081E-10
Pkp1	plakophilin 1	12.110	4.109E-29
Meltf	melanotransferrin	11.132	8.000E-23
Car15	carbonic anhydrase 15	10.550	2.654E-06
Slc26a4	solute carrier family 26, member 4	10.010	3.769E-18
Bcat1	branched chain aminotransferase 1, cytosolic	9.839	2.746E-14
Ccn5	cellular communication network factor 5	8.863	7.652E-35
Dio3	deiodinase, iodothyronine type III	8.245	3.347E-06
Trpm2	transient receptor potential cation channel, subfamily M, member 2	7.087	8.723E-19
Kcnq3	potassium voltage-gated channel, subfamily Q, member 3	7.053	2.946E-05
Rph3a	rabphilin 3A	5.971	7.179E-05
Sphk1	sphingosine kinase 1	5.723	1.925E-20
Gdf15	growth differentiation factor 15	5.619	2.994E-25
Grem1	gremlin 1, DAN family BMP antagonist	5.596	1.409E-13
Scn5a	sodium channel, voltage-gated, type V, alpha	5.352	3.122E-08
Adora2b	adenosine A2b receptor	5.313	0.0003
Ms4a14	membrane-spanning 4-domains, subfamily A, member 14, transcript variant X2	5.296	2.191E-05
Gpr176	G protein-coupled receptor 176	5.238	5.041E-09
Stra6	stimulated by retinoic acid gene 6	5.210	2.391E-09
Gdf6	growth differentiation factor 6	5.147	4.846E-05
Pimreg	PICALM interacting mitotic regulator	5.140	7.797E-08
Cenpf	centromere protein F	5.041	3.468E-14
Plk1	Polo-like kinase 1	5.003	9.373E-10
Eppk1	epiplakin 1	4.894	1.126E-29
Lgals3	lectin, galactose binding, soluble 3	4.843	9.115E-11
Iqgap3	IQ motif containing GTPase-activating protein 3	4.821	4.179E-33
Nek2	NIMA (never in mitosis gene a)-related expressed kinase 2	4.697	4.649E-05
Psrc1	proline/serine-rich coiled-coil 1	4.684	8.398E-10
Cep55	centrosomal protein 55	4.646	2.568E-07

Fold changes between the TSH and Empty group in TPM of genes are represented. Statistical analyses were performed with the Wald test.

exhibited similar serum fT3 levels to those of hypothyroid mice treated with 0.1 μg/mL of LT3.[34] Considering that hypothyroid mice treated with 1 μg/mL of LT3 displayed more severe phenotypes,[34] the severity of thyrotoxicosis in our hyperthyroid mice appears to be mild to moderate. However, our hyperthyroid mice differ from models based on exogenous administrations due to their increased secretion of thyroid hormones. Meanwhile, species difference is an important consideration. For example, hyperthyroidism in humans is typically associated with body weight reduction, whereas our hyperthyroid mice gained body weight. The molecular features of the thyroid gland, which is a focal point of this study, may also differ between mice and humans.

Our hyperthyroid mouse, generated by overexpressing human TSH, has the following merits compared to previous models. First, hyperthyroidism consistently and promptly developed at 1 day after hydrodynamic gene delivery and persisted for at least 4 weeks. Second, we can validate and monitor TSH overexpression by measuring serum human TSH levels. Compared with human TSH, murine TSH levels are difficult to measure.[35] The kit we used could detect overexpression of human TSH. There was significant cross-reaction with endogenous murine TSH, as seen in the results of the Empty group. Activation of murine TSHR by overexpression of human TSH was verified by an increase in the thyroidal cAMP content. Third, the strategy of acquired generation can avoid bias arising during growth periods. Lastly, we can cause hyperthyroidism in various mice because one hydrodynamic injection of the same plasmid vectors is just needed. We believe our technique of hyperthyroidism induction can be also useful in other investigations.

Hydrodynamic gene delivery is a technique for *in vivo* transfection. Prolonged overexpression is obtained by using a pLIVE vector backbone. In a previous study, we applied this system to increase circulating levels of C-type natriuretic peptide and verified the prolonged increase even at 4 weeks after transfection.[25] Attempts to increase circulating protein levels with hydrodynamic gene delivery using pLIVE vectors were performed for fibroblast growth factor 21[36,37] and soluble T-cadherin.[38] Kwon

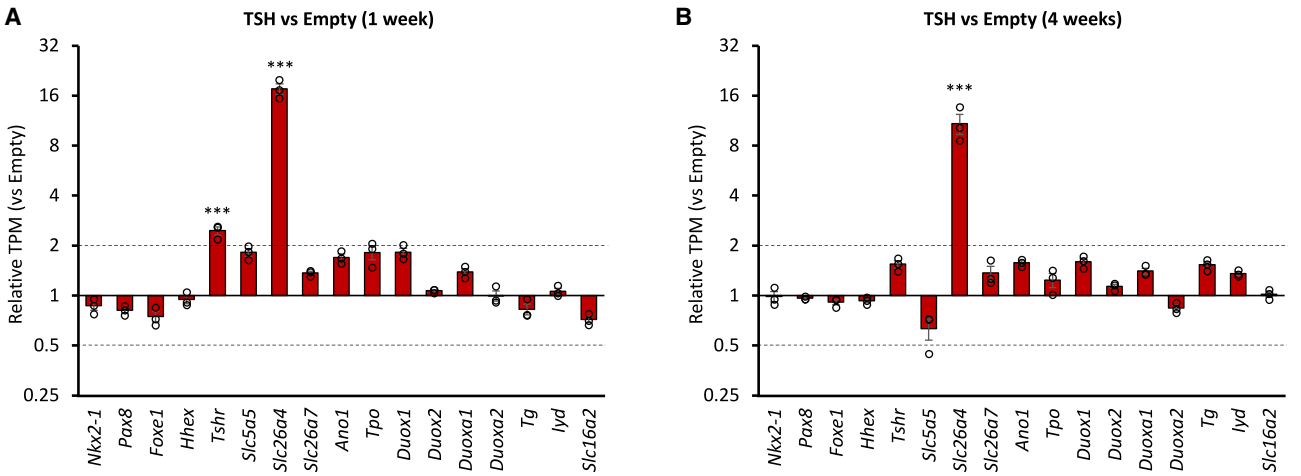

Figure 7. Summary of RNA-seq regarding thyroidal genes

(A and B) Results at 1 week (A) and 4 weeks (B) after hydrodynamic gene delivery. See Tables S1 and S2 for the source data. Data are represented as fold changes between the TSH group and the Empty group in transcripts per kilobase million (TPM) of genes. The Wald test was used to compare TPM of genes from each cohort. ***$p < 0.001$.

et al. demonstrated that the elevation of plasma fibroblast growth factor 21 levels was maintained at 100 days after hydrodynamic injection.[37] Thus, our hyperthyroid mice are also expected to maintain high serum TSH levels for several months. As the *TSHR* knock-in mice developed papillary thyroid carcinomas at 12 months of age,[33] long-term observations of our hyperthyroid mice may yield interesting findings.

It should be noted that our hyperthyroid mouse model does not fully mimic Graves' disease. Lymphocytic infiltration was not observed in the thyroid glands of our hyperthyroid mice. In addition to immunological changes, activation of TSHR by TSH receptor antibodies in Graves' disease may result in different signaling from that induced by TSH overexpression. Furthermore, post-translational modifications of TSH overexpressed with pLIVE vectors may differ from those of endogenous TSH. Tissue-specific glycosylation of TSH is important for its activity.[39] It is possible that overexpressed TSH and endogenous TSH differentially alter TSHR signaling. Although TSH-secreting pituitary neuroendocrine tumors are similar to our hyperthyroid mice in terms of ectopic TSH secretion, careful interpretation is needed due to differences in post-translational modifications and orders of magnitude in serum TSH levels.

Transcriptome analyses of the thyroid gland focusing on thyroid dysfunction have been limited to reports on a murine model of Graves' disease[40] and a murine model of iodine treatment.[41] To the best of our knowledge, there have been no clinical reports about the thyroid transcriptome of patients with hyperthyroidism. In the present study, our hyperthyroid mice provided valuable information on the molecular signature of hyperthyroidism. First, we investigated mechanisms of MMI action on hyperthyroidism but could find few changes in the thyroid transcriptome. In other words, MMI seemed to attenuate hyperthyroidism regardless of transcriptional regulation. PTU treatment also did not alter thyroidal gene expression. ATDs such as MMI and PTU inhibit TPO activity.[42,43] Our results reinforce a conventional theory that ATDs decrease thyroid hormone secretion by inhibiting TPO.[44] Meanwhile, we set the MMI concentration to equalize serum fT4 levels of the Empty and TSH-MMI groups. Although serum fT4 levels differed between the TSH and TSH-MMI groups, they had similar transcriptome patterns. Taken together, transcriptome changes did not seem to depend on serum thyroid hormone levels, but on TSHR signaling. Although serum fT3 levels were not decreased in the TSH-MMI group, we believe that the effects of MMI on the thyroid glands were evident, as MMI administration resulted in decreased serum fT4 levels, reduced goiter size, and smaller follicle size. However, higher concentrations of MMI and PTU may lead to transcriptome changes.

GO enrichment analyses of TSH overexpression at 1 week shed light on the cell cycle (Figure 5A). *Cdkn3*, *Plk1*, and *Ccnb1,* which are related to the cell cycle, were listed among the top 30 upregulated genes at 1 week (Table 1). It is well known that TSH activates cell proliferation,[11] which might be involved in cell cycle progression.[45,46] Meanwhile, changes related to the cell cycle were not seen in GO terms or the top 30 upregulated genes at 4 weeks (Figure 6 and Table 2). Instead, we noticed the phosphatidylinositol 3-kinase (PI3K)/Akt pathway and Ras-related protein 1 (Rap1) pathway among KEGG terms (Figures 5D and 6D). Previous studies have verified that TSHR signaling includes the activation of PI3K and consequent phosphorylation of Akt.[47–49] TSHR signaling directly activates the phospholipase C cascade as well as the cAMP/PKA pathway via G proteins,[12,13] but how these mechanisms contribute to PI3K/Akt pathway activation is unclear. PI3K inhibition attenuates the proliferative effects of TSH,[49,50] which support the involvement of the PI3K/Akt pathway in goiter development in our hyperthyroid mice.

On the other hand, Rap1 induction by TSH through both PKA-dependent and PKA-independent pathways has been reported.[51,52] Rap1 is known as an activator of mitogen-activated protein kinase signaling through BRAF activation.[53] A similar action of Rap1 was observed in the FRTL5 rat thyroid cell line.[54]

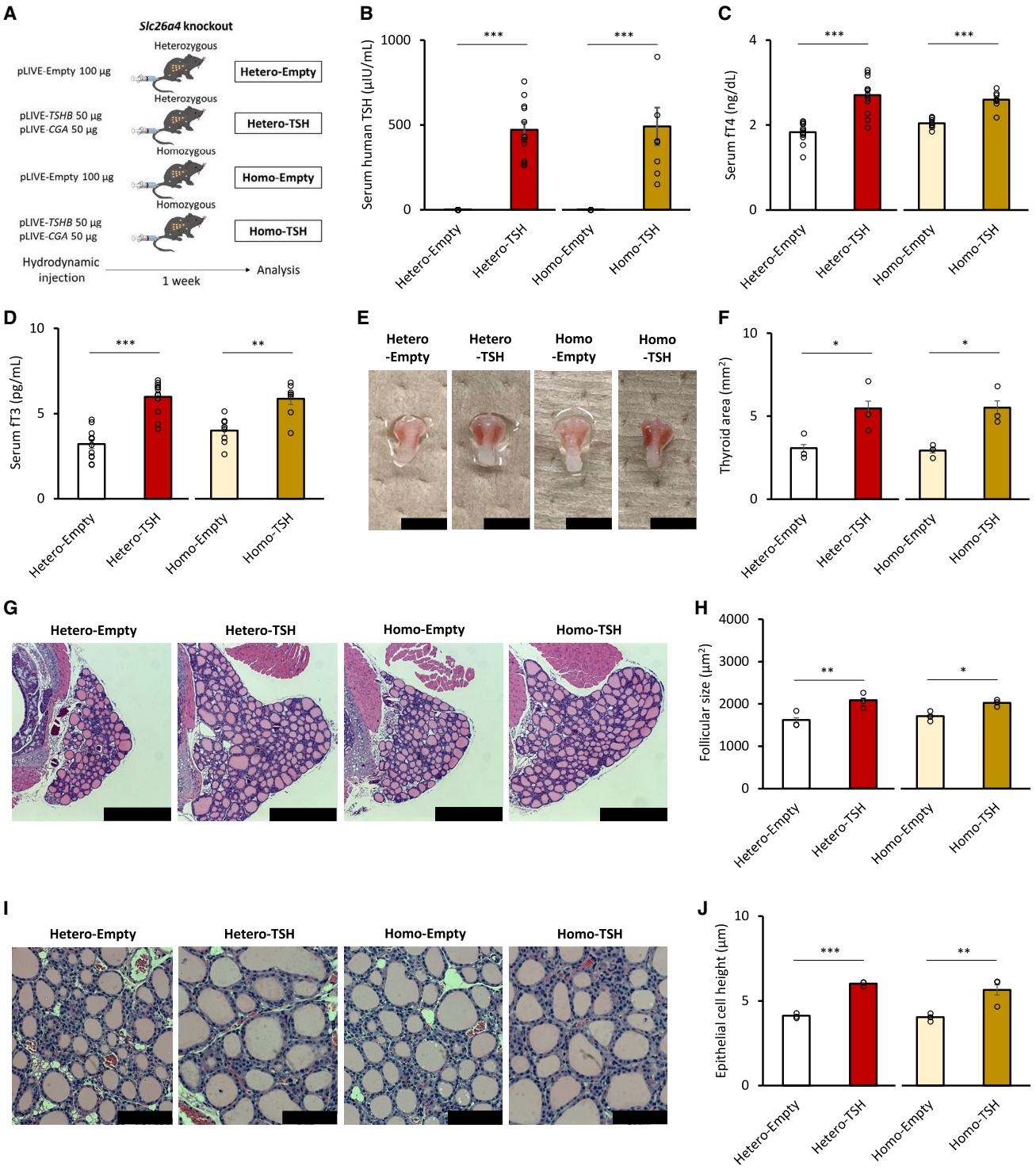

Figure 8. Phenotypes of *Slc26a4* knockout mice overexpressing TSH

(A) Schema for the experimental design.

(B–D) Serum levels of thyroid hormones. Hetero-Empty, Hetero-TSH, n = 12 each; Homo-Empty, Homo-TSH, n = 8 each.

(E) Gross appearance of thyroid glands. The black scale bar is 5 mm.

(F) Thyroid gland size measured based on photographs. n = 3 each.

(G) Histological images of thyroid glands with hematoxylin and eosin staining at 50× magnification. The black scale bar is 500 μm.

(legend continued on next page)

Given that the induction of a gain-of-function BRAF mutation enlarged murine thyroid glands by promoting mitosis,[55] we believe that Rap1 signaling also contributed to the goiter development of our hyperthyroid mice.

From another perspective, antioxidant responses induced by TSHR signaling are highlighted. We observed transcriptional upregulation of antioxidant genes such as *Srxn1*, *Txnrd1*, and *Upk3bl*. Previous reports demonstrated that oxidative stress caused by iodide overload is accompanied by the upregulation of these antioxidant genes.[31,41] Oxidative stress frequently causes DNA damage and modifications in the thyroid gland.[56] During thyroid hormone synthesis, oxidative stress is induced by high amounts of oxidant hydrogen peroxide generated to oxidize iodide and iodinate thyroglobulin.[31] In this context, hyperthyroidism can augment oxidative stress in the thyroid gland, which appears to induce antioxidant responses in our hyperthyroid mice. Subsequently, we noticed that such antioxidant responses could develop goiter. The keap1-Nrf2 pathway is an important mediator of antioxidant responses in the thyroid gland.[31,57] As patients with *KEAP1* variants and *Keap1* knockdown mice develop a goiter,[58–60] augmentation of antioxidant responses can contribute to the size and histological changes in the thyroid glands of our hyperthyroid mice. Regulation of antioxidant responses, including the Keap1-Nrf2 pathway, is a possible strategy to prevent goiter development in hyperthyroidism.

Furthermore, our GO enrichment analyses revealed additional noteworthy points. First, we found that GO terms related to the extracellular matrix were enriched. Thyroid eye disease (TED) is the most common extrathyroidal manifestation of Graves' disease, and TSHR stimulation in orbital tissue plays a major role in its pathophysiology. The characteristic features of TED arise from inflammation and extracellular matrix expansion in the orbital tissue.[61] Notably, the accumulation of hyaluronic acid is well documented, and we identified an enriched term, "hyaluronic acid binding," along with an upregulation of the *Acan* gene coding for aggrecan (with a fold change of 8.158 at 1 week). Our thyroid transcriptome data may enhance our understanding of the role of TSHR signaling in the pathophysiology of TED. Second, GO terms related to the microtubule were enriched at both 1 week and 4 weeks (Tables S3 and S4). These terms include genes coding for kinesins superfamily proteins: *Kif2c*, *Kif4*, *Kif11*, *Kif14*, *Kif15*, *Kif18a*, *Kif18b*, *Kif20a*, *Kiaf20b*, *Kif22*, *Kif23*, *Kifc1*, and *Kifc5b* were upregulated at 1 week (Table S1): *Kif1a*, *Kif4*, *Kif11*, *Kif14*, *Kif20a*, *Kif22*, *Kif23*, *Kifc1*, and *Kifc5b* were upregulated at 4 weeks (Table S2). Associations between thyroid cancer and kinesins have been studied,[62,63] and interestingly, *Kif3a* knockout mice exhibited mild hypothyroidism.[64] The role of kinesins in hyperthyroidism is also an intriguing area of focus.

We also elucidated iodothyronine deiodinases. D1 role in hyperthyroidism due to Graves' disease was suggested by therapeutic effects of PTU, a D1 inhibitor,[65] and increased D1 expression by TSH in the FRTL5 rat thyroid cell line.[66] A recent report demonstrated that *Dio3* mRNA was increased in the thyroid gland of Graves' disease model mice and that the increase in Dio3 mRNA correlated with rT3 abundance.[40] In the present study, we only confirmed *Dio2* upregulation, but this significance requires further elucidation because there are species-specific differences in D2 expression in the thyroid gland.[67] It should also be noted that mRNA levels of *Dio2* and *Dio3* seemed to be much lower than that of *Dio1*, as shown by TPM in RNA-seq analyses.

We also examined whether SLC26A4 played a significant role in the development of hyperthyroidism because its encoding gene, *Slc26a4*, was exclusively upregulated among thyroidal genes with TSH overexpression. Pesce et al. reported that TSH and forskolin regulate SLC26A4 abundance in the plasma membrane of the PCCL-3 rat thyroid cell line, suggesting the involvement of the cAMP/PKA pathway in *Slc26a4* upregulation.[68] Administration of sodium iodide and thyroid hormones did not increase *Slc26a4* mRNA levels, whereas *Nkx2-1* overexpression increased *Slc26a4* mRNA levels in the FRTL5 rat thyroid cell line.[69,70] Our transcriptome data showed that *Nkx2-1* expression did not change at either 1 week or 4 weeks. *Slc26a4* mRNA was also upregulated in a murine model of Graves' disease.[40] In addition, examinations of human thyroid tissues have revealed that SLC26A4 expression is augmented in Graves' disease.[71,72] Hypothyroidism due to loss-of-function mutations in *SLC26A4* occurs in Pendred syndrome,[32] but the effects of increased levels of SLC26A4 on thyroid function have not been clarified.

In this context, we generated and analyzed *Slc26a4* knockout mice with hyperthyroidism that did not have increases in *Slc26a4* mRNA expression with TSH overexpression. SLC26A4 depletion did not affect their thyroid function and morphology. We excluded compensative changes in the gene expression of components necessary for thyroid hormone secretion including *SLC5A5*, *ANO1*, *SLC26A7*, and other iodine transporters.[73–75] As *Slc5a5* mRNA was downregulated only in heterozygous *Slc26a4* knockout mice at 1 week, we addressed this bias by results at 3 days that both heterozygous and homozygous mice exhibited similar profiles in thyroidal gene expression. This finding might be explained with a report that *Slc26a7* knockout mice develop hypothyroidism, but *Slc26a4* knockout mice do not.[76] As seen in our western blot results, SLC26A4 protein might be slightly expressed and not play a significant role in the murine thyroid gland.

SLC26A4 did not seem to be involved in hyperthyroidism, which was interesting because our mice developed hyperthyroidism without any changes in known thyroidal genes. In the process of developing hyperthyroidism through the activation of TSHR signaling, a number of genes should be regulated because PKA generally phosphorylates cAMP response element binding protein and regulates its target genes.[77,78] In other words, DEGs in our datasets might include candidate genes that have not yet been identified as regulators of thyroid function. Changes in the structure of the thyroid gland, such as size and number of follicles, may also be involved in hyperthyroidism.

(H) Mean follicle size is calculated based on histological images. $n = 3$ each.

(I) Histological images of thyroid glands with hematoxylin and eosin staining at 200× magnification. The black scale bar is 100 μm.

(J) Epithelial cell height is measured based on histological images. $n = 3$ each. Data are represented as means ± SEM. Statistical analyses were performed using Student's *t*-test to compare the Empty and TSH groups for each knockout mouse. $^{*}p < 0.05$, $^{**}p < 0.01$, and $^{***}p < 0.001$.

We hope that our RNA-seq datasets (Tables S1 and S2) will provide inspiration to other researchers. We manually reviewed the datasets and found the following suggestions. *Lgals3*, a gene encoding galectin-3, was upregulated. Galectin-3 is a well-known marker for differentiated thyroid cancer.[79] Considering that TSH suppression therapy is effective against differentiated thyroid cancer, a relationship between TSHR signaling and galectin-3 is reasonable. Moreover, *Gdf15* was seen among the top 30 genes at both 1 and 4 weeks. Growth differentiation factor 15 (GDF15) is associated with various endocrine conditions.[80] Patients with hyperthyroidism have high serum GDF15 levels,[81] as well as patients with papillary thyroid carcinoma.[82] In addition, papillary thyroid carcinomas often express GDF15.[82] As for hyperthyroidism, we are interested in *Siglec1* upregulation. Hashimoto et al. reported that patients who experience a relapse of Graves' disease have high *SIGLEC1* mRNA levels in peripheral leukocytes.[83] The role of sialic acid-binding immunoglobulin-like lectin-1 (SIGLEC1) in the thyroid gland has not been clarified. Perspectives on TSHR signaling might contribute to greater understanding of thyroid biology. We provide readers with valuable information on the thyroid transcriptome; lists of significant terms in enrichment analyses (Tables S3, S4, S5, and S6), a list of genes upregulated at both 1 and 4 weeks (Table S7), and lists of DEGs including data at another week (Tables S8 and S9).

In conclusion, we generated a mouse model of hyperthyroidism based on TSH overexpression to clarify the molecular landscape of TSHR signaling in a hyperthyroid state. Although MMI administration caused few changes in the thyroid transcriptome, TSH overexpression induced drastic changes. As *Slc26a4* was exclusively upregulated among known thyroidal genes with TSH overexpression, we verified the significance of *Slc26a4* in hyperthyroidism based on analyses of *Slc26a4* knockout mice. As a result, *Slc26a4* knockout mice developed hyperthyroidism similar to control mice. It is possible that unrecognized genes are involved in the development of hyperthyroidism. We hope the transcriptome datasets presented here will contribute to future research.

Limitations of the study

The present study has several limitations. First, the TSH overexpressed in our system might not have post-translational modifications because it was predominantly produced in the liver,[26] not the pituitary gland, which is different from physiological TSH secretion. Likewise, TSHR-stimulating antibodies in Graves' disease might affect TSHR signaling differently. Second, differences in thyroid physiology between species should be considered. Although thyroidal genes were rarely changed with TSH overexpression in our mice, the human thyroid gland might undergo different changes. Analyses using human thyroid tissues or organoids are needed to address this limitation. Third, we analyzed the thyroid transcriptome using bulk RNA-seq, which included C cells and the parathyroid glands as well as follicular epithelial cells due to technical difficulties. We actually found decreases in their respective marker genes, *Calca* and *Pth*, with TSH overexpression (Tables S1 and S2). Therefore, interpretation of downregulated genes might be difficult. Single-cell analysis or other techniques are required for further investigation.

RESOURCE AVAILABILITY

Lead contact

Further information and requests for resources and reagents should be directed to and will be fulfilled by the lead contact, Ichiro Yamauchi (ichiroy@kuhp.kyoto-u.ac.jp).

Materials availability

Material generated in this study will be shared by the lead contact upon request.

Data and code availability

- RNA-seq data have been deposited at GEO and have been publicly available. The accession number is listed in the key resources table. The analyzed datasets are provided in Tables S1, S2, S3, S4, S5, S6, S7, S8, and S9.
- This paper does not report the original code.
- Any additional information required to reanalyze the data reported in this paper is available from the lead contact upon request.

ACKNOWLEDGMENTS

This work was supported by JSPS KAKENHI grants (Number 19K18006, 20K17508, 22K16394, and 23K15410) and by grants from Uehara Memorial Foundation, Takeda Science Foundation, and Japan Foundation for Applied Enzymology.

AUTHOR CONTRIBUTIONS

Conceptualization, IY; experiments using C57BL/6J mice, IY, TS, and TH; experiments using *Slc26a4* knockout mice, IY, TS, AY, TK, and YK; experiments for revision, IY, TS, TH, SK, and AS; data analyses, IY, TS, TH, SK, DK, HF, KO, YU, TF, and DT; funding acquisition, IY and SY; supervision, AY and NI. IY drafted the article, and all authors reviewed, edited, and approved the article.

DECLARATION OF INTERESTS

The authors declare no competing financial interests.

STAR★METHODS

Detailed methods are provided in the online version of this paper and include the following:

- KEY RESOURCES TABLE
- EXPERIMENTAL MODEL AND STUDY PARTICIPANT DETAILS
  - Animals
- METHOD DETAILS
  - Plasmid construction
  - Hydrodynamic gene delivery and MMI administration
  - Sample collection
  - Thyroid morphological analysis
  - Measurement of thyroid hormones and cAMP
  - RNA extraction, RT-PCR, and quantitative RT-PCR
  - RNA-seq and bioinformatics analysis
  - Western blotting
- QUANTIFICATION AND STATISTICAL ANALYSIS

SUPPLEMENTAL INFORMATION

Supplemental information can be found online at https://doi.org/10.1016/j.isci.2024.111565.

Received: December 21, 2023
Revised: July 6, 2024
Accepted: December 6, 2024
Published: December 10, 2024

REFERENCES

1. Davies, T.F., Andersen, S., Latif, R., Nagayama, Y., Barbesino, G., Brito, M., Eckstein, A.K., Stagnaro-Green, A., and Kahaly, G.J. (2020). Graves' disease. Nat. Rev. Dis. Prim. *6*, 52. https://doi.org/10.1038/s41572-020-0184-y.
2. Ross, D.S., Burch, H.B., Cooper, D.S., Greenlee, M.C., Laurberg, P., Maia, A.L., Rivkees, S.A., Samuels, M., Sosa, J.A., Stan, M.N., and Walter, M.A. (2016). 2016 American Thyroid Association Guidelines for Diagnosis and Management of Hyperthyroidism and Other Causes of Thyrotoxicosis. Thyroid *26*, 1343–1421. https://doi.org/10.1089/thy.2016.0229.
3. Burch, H.B., Burman, K.D., and Cooper, D.S. (2012). A 2011 survey of clinical practice patterns in the management of Graves' disease. J. Clin. Endocrinol. Metab. *97*, 4549–4558. https://doi.org/10.1210/jc.2012-2802.
4. Alexander, E.K., Pearce, E.N., Brent, G.A., Brown, R.S., Chen, H., Dosiou, C., Grobman, W.A., Laurberg, P., Lazarus, J.H., Mandel, S.J., et al. (2017). 2017 Guidelines of the American Thyroid Association for the Diagnosis and Management of Thyroid Disease During Pregnancy and the Postpartum. Thyroid *27*, 315–389. https://doi.org/10.1089/thy.2016.0457.
5. Kahaly, G.J., Bartalena, L., Hegedüs, L., Leenhardt, L., Poppe, K., and Pearce, S.H. (2018). 2018 European Thyroid Association Guideline for the Management of Graves' Hyperthyroidism. Eur. Thyroid J. *7*, 167–186. https://doi.org/10.1159/000490384.
6. Bahn Chair, R.S., Burch, H.B., Cooper, D.S., Garber, J.R., Greenlee, M.C., Klein, I., Laurberg, P., McDougall, I.R., Montori, V.M., Rivkees, S.A., et al. (2011). Hyperthyroidism and other causes of thyrotoxicosis: management guidelines of the American Thyroid Association and American Association of Clinical Endocrinologists. Thyroid *21*, 593–646. https://doi.org/10.1089/thy.2010.0417.
7. Parma, J., Duprez, L., Van Sande, J., Cochaux, P., Gervy, C., Mockel, J., Dumont, J., and Vassart, G. (1993). Somatic mutations in the thyrotropin receptor gene cause hyperfunctioning thyroid adenomas. Nature *365*, 649–651. https://doi.org/10.1038/365649a0.
8. Führer, D., Holzapfel, H.P., Wonerow, P., Scherbaum, W.A., and Paschke, R. (1997). Somatic mutations in the thyrotropin receptor gene and not in the Gs alpha protein gene in 31 toxic thyroid nodules. J. Clin. Endocrinol. Metab. *82*, 3885–3891. https://doi.org/10.1210/jcem.82.11.4382.
9. Georgopoulos, N.A., Sykiotis, G.P., Sgourou, A., Papachatzopoulou, A., Markou, K.B., Kyriazopoulou, V., Papavassiliou, A.G., and Vagenakis, A.G. (2003). Autonomously functioning thyroid nodules in a former iodine-deficient area commonly harbor gain-of-function mutations in the thyrotropin signaling pathway. Eur. J. Endocrinol. *149*, 287–292. https://doi.org/10.1530/eje.0.1490287.
10. Gozu, H.I., Bircan, R., Krohn, K., Müller, S., Vural, S., Gezen, C., Sargin, H., Yavuzer, D., Sargin, M., Cirakoglu, B., and Paschke, R. (2006). Similar prevalence of somatic TSH receptor and Gsalpha mutations in toxic thyroid nodules in geographical regions with different iodine supply in Turkey. Eur. J. Endocrinol. *155*, 535–545. https://doi.org/10.1530/eje.1.02253.
11. Vassart, G., and Dumont, J.E. (1992). The thyrotropin receptor and the regulation of thyrocyte function and growth. Endocr. Rev. *13*, 596–611. https://doi.org/10.1210/edrv-13-3-596.
12. Laurent, E., Mockel, J., Van Sande, J., Graff, I., and Dumont, J.E. (1987). Dual activation by thyrotropin of the phospholipase C and cyclic AMP cascades in human thyroid. Mol. Cell. Endocrinol. *52*, 273–278. https://doi.org/10.1016/0303-7207(87)90055-4.
13. Van Sande, J., Dequanter, D., Lothaire, P., Massart, C., Dumont, J.E., and Erneux, C. (2006). Thyrotropin stimulates the generation of inositol 1,4,5-trisphosphate in human thyroid cells. J. Clin. Endocrinol. Metab. *91*, 1099–1107. https://doi.org/10.1210/jc.2005-1324.
14. Van Heuverswyn, B., Streydio, C., Brocas, H., Refetoff, S., Dumont, J., and Vassart, G. (1984). Thyrotropin controls transcription of the thyroglobulin gene. Proc. Natl. Acad. Sci. USA *81*, 5941–5945. https://doi.org/10.1073/pnas.81.19.5941.
15. Nagayama, Y., Yamashita, S., Hirayu, H., Izumi, M., Uga, T., Ishikawa, N., Ito, K., and Nagataki, S. (1989). Regulation of thyroid peroxidase and thyroglobulin gene expression by thyrotropin in cultured human thyroid cells. J. Clin. Endocrinol. Metab. *68*, 1155–1159. https://doi.org/10.1210/jcem-68-6-1155.
16. Saito, T., Endo, T., Kawaguchi, A., Ikeda, M., Nakazato, M., Kogai, T., and Onaya, T. (1997). Increased expression of the Na+/I- symporter in cultured human thyroid cells exposed to thyrotropin and in Graves' thyroid tissue. J. Clin. Endocrinol. Metab. *82*, 3331–3336. https://doi.org/10.1210/jcem.82.10.4269.
17. Jang, D., Morgan, S.J., Klubo-Gwiezdzinska, J., Banga, J.P., Neumann, S., and Gershengorn, M.C. (2020). Thyrotropin, but Not Thyroid-Stimulating Antibodies, Induces Biphasic Regulation of Gene Expression in Human Thyrocytes. Thyroid *30*, 270–276. https://doi.org/10.1089/thy.2019.0418.
18. Levy, O., Dai, G., Riedel, C., Ginter, C.S., Paul, E.M., Lebowitz, A.N., and Carrasco, N. (1997). Characterization of the thyroid Na+/I- symporter with an anti-COOH terminus antibody. Proc. Natl. Acad. Sci. USA *94*, 5568–5573. https://doi.org/10.1073/pnas.94.11.5568.
19. Eng, P.H., Cardona, G.R., Fang, S.L., Previti, M., Alex, S., Carrasco, N., Chin, W.W., and Braverman, L.E. (1999). Escape from the acute Wolff-Chaikoff effect is associated with a decrease in thyroid sodium/iodide symporter messenger ribonucleic acid and protein. Endocrinology *140*, 3404–3410. https://doi.org/10.1210/endo.140.8.6893.
20. McLachlan, S.M., Nagayama, Y., and Rapoport, B. (2005). Insight into Graves' hyperthyroidism from animal models. Endocr. Rev. *26*, 800–832. https://doi.org/10.1210/er.2004-0023.
21. Zhang, M., Jiang, W., Lu, G., Wang, R., Lv, Z., and Li, D. (2022). Insight Into Mouse Models of Hyperthyroidism. Front. Endocrinol. *13*, 929750. https://doi.org/10.3389/fendo.2022.929750.
22. Liu, F., Song, Y., and Liu, D. (1999). Hydrodynamics-based transfection in animals by systemic administration of plasmid DNA. Gene Ther. *6*, 1258–1266. https://doi.org/10.1038/sj.gt.3300947.
23. Wondisford, F.E., Radovick, S., Moates, J.M., Usala, S.J., and Weintraub, B.D. (1988). Isolation and characterization of the human thyrotropin beta-subunit gene. Differences in gene structure and promoter function from murine species. J. Biol. Chem. *263*, 12538–12542. https://doi.org/10.1016/S0021-9258(19)75737-8.
24. Fiddes, J.C., and Goodman, H.M. (1981). The gene encoding the common alpha subunit of the four human glycoprotein hormones. J. Mol. Appl. Genet. *1*, 3–18.
25. Yamashita, T., Fujii, T., Yamauchi, I., Ueda, Y., Hirota, K., Kanai, Y., Yasoda, A., and Inagaki, N. (2020). C-Type Natriuretic Peptide Restores Growth Impairment Under Enzyme Replacement in Mice With Mucopolysaccharidosis VII. Endocrinology *161*, bqaa008. https://doi.org/10.1210/endocr/bqaa008.
26. Yamauchi, I., Sakane, Y., Yamashita, T., Hakata, T., Sugawa, T., Fujita, H., Okamoto, K., Taura, D., Hirota, K., Ueda, Y., et al. (2022). Thyroid hormone economy in mice overexpressing iodothyronine deiodinases. Faseb. J. *36*, e22141. https://doi.org/10.1096/fj.202101288RR.
27. Yamauchi, I., Yamashita, T., Sugawa, T., Tagami, T., Hanaoka, I., Usui, T., Hirota, K., Hakata, T., Ueda, Y., Fujii, T., et al. (2022). Bezafibrate induces hypothyroidism in a patient with resistance to thyroid hormone β due to a G347R variant. Clin. Endocrinol. *96*, 236–245. https://doi.org/10.1111/cen.14591.
28. de Assis, L.V.M., Harder, L., Lacerda, J.T., Parsons, R., Kaehler, M., Cascorbi, I., Nagel, I., Rawashdeh, O., Mittag, J., and Oster, H. (2022). Rewiring of liver diurnal transcriptome rhythms by triiodothyronine (T(3)) supplementation. Elife *11*, e79405. https://doi.org/10.7554/eLife.79405.
29. de Assis, L.V.M., Harder, L., Lacerda, J.T., Parsons, R., Kaehler, M., Cascorbi, I., Nagel, I., Rawashdeh, O., Mittag, J., and Oster, H. (2024). Tuning of liver circadian transcriptome rhythms by thyroid hormone state in male mice. Sci. Rep. *14*, 640. https://doi.org/10.1038/s41598-023-50374-z.

30. Wu, Z., Martinez, M.E., and Hernandez, A. (2024). Mice lacking DIO3 exhibit sex-specific alterations in circadian patterns of corticosterone and gene expression in metabolic tissues. BMC Mol. Cell Biol. *25*, 11. https://doi.org/10.1186/s12860-024-00508-6.

31. Ziros, P.G., Habeos, I.G., Chartoumpekis, D.V., Ntalampyra, E., Somm, E., Renaud, C.O., Bongiovanni, M., Trougakos, I.P., Yamamoto, M., Kensler, T.W., et al. (2018). NFE2-Related Transcription Factor 2 Coordinates Antioxidant Defense with Thyroglobulin Production and Iodination in the Thyroid Gland. Thyroid *28*, 780–798. https://doi.org/10.1089/thy.2018.0018.

32. Everett, L.A., Glaser, B., Beck, J.C., Idol, J.R., Buchs, A., Heyman, M., Adawi, F., Hazani, E., Nassir, E., Baxevanis, A.D., et al. (1997). Pendred syndrome is caused by mutations in a putative sulphate transporter gene (PDS). Nat. Genet. *17*, 411–422. https://doi.org/10.1038/ng1297-411.

33. Jaeschke, H., Undeutsch, H., Patyra, K., Löf, C., Eszlinger, M., Khalil, M., Jännäri, M., Makkonen, K., Toppari, J., Zhang, F.P., et al. (2018). Hyperthyroidism and Papillary Thyroid Carcinoma in Thyrotropin Receptor D633H Mutant Mice. Thyroid *28*, 1372–1386. https://doi.org/10.1089/thy.2018.0041.

34. Yamauchi, I., Hakata, T., Ueda, Y., Sugawa, T., Omagari, R., Teramoto, Y., Nakayama, S.F., Nakajima, D., Kubo, T., and Inagaki, N. (2023). TRIAC disrupts cerebral thyroid hormone action via negative feedback and heterogenous distribution among organs. iScience *26*, 107135. https://doi.org/10.1016/j.isci.2023.107135.

35. Bianco, A.C., Anderson, G., Forrest, D., Galton, V.A., Gereben, B., Kim, B.W., Kopp, P.A., Liao, X.H., Obregon, M.J., Peeters, R.P., et al. (2014). American Thyroid Association Guide to investigating thyroid hormone economy and action in rodent and cell models. Thyroid *24*, 88–168. https://doi.org/10.1089/thy.2013.0109.

36. Gao, M., Ma, Y., Cui, R., and Liu, D. (2014). Hydrodynamic delivery of FGF21 gene alleviates obesity and fatty liver in mice fed a high-fat diet. J. Contr. Release *185*, 1–11. https://doi.org/10.1016/j.jconrel.2014.03.047.

37. Kwon, M.M., O'Dwyer, S.M., Baker, R.K., Covey, S.D., and Kieffer, T.J. (2015). FGF21-Mediated Improvements in Glucose Clearance Require Uncoupling Protein 1. Cell Rep. *13*, 1521–1527. https://doi.org/10.1016/j.celrep.2015.10.021.

38. Okita, T., Kita, S., Fukuda, S., Fukuoka, K., Kawada-Horitani, E., Iioka, M., Nakamura, Y., Fujishima, Y., Nishizawa, H., Kawamori, D., et al. (2022). Soluble T-cadherin promotes pancreatic β-cell proliferation by upregulating Notch signaling. iScience *25*, 105404. https://doi.org/10.1016/j.isci.2022.105404.

39. Ikegami, K., Liao, X.H., Hoshino, Y., Ono, H., Ota, W., Ito, Y., Nishiwaki-Ohkawa, T., Sato, C., Kitajima, K., Iigo, M., et al. (2014). Tissue-specific posttranslational modification allows functional targeting of thyrotropin. Cell Rep. *9*, 801–810. https://doi.org/10.1016/j.celrep.2014.10.006.

40. Uchida, T., Shimamura, M., Taka, H., Kaga, N., Miura, Y., Nishida, Y., Nagayama, Y., and Watada, H. (2023). The Effect of Long-Term Inorganic Iodine on Intrathyroidal Iodothyronine Content and Gene Expression in Mice with Graves' Hyperthyroidism. Thyroid *33*, 330–337. https://doi.org/10.1089/thy.2022.0496.

41. Chartoumpekis, D.V., Ziros, P.G., Georgakopoulos-Soares, I., Smith, A.A.T., Marques, A.C., Ibberson, M., A Kopp, P., Habeos, I., Trougakos, I.P., Khoo, N.K.H., and Sykiotis, G.P. (2020). The Transcriptomic Response of the Murine Thyroid Gland to Iodide Overload and the Role of the Nrf2 Antioxidant System. Antioxidants *9*, 884. https://doi.org/10.3390/antiox9090884.

42. Davidson, B., Soodak, M., Neary, J.T., Strout, H.V., Kieffer, J.D., Mover, H., and Maloof, F. (1978). The irreversible inactivation of thyroid peroxidase by methylmercaptoimidazole, thiouracil, and propylthiouracil *in vitro* and its relationship to *in vivo* findings. Endocrinology *103*, 871–882. https://doi.org/10.1210/endo-103-3-871.

43. Taurog, A., and Dorris, M.L. (1989). A reexamination of the proposed inactivation of thyroid peroxidase in the rat thyroid by propylthiouracil. Endocrinology *124*, 3038–3042. https://doi.org/10.1210/endo-124-6-3038.

44. Wiersinga, W.M., Poppe, K.G., and Effraimidis, G. (2023). Hyperthyroidism: aetiology, pathogenesis, diagnosis, management, complications, and prognosis. Lancet Diabetes Endocrinol. *11*, 282–298. https://doi.org/10.1016/s2213-8587(23)00005-0.

45. Lamy, F., Roger, P., Lecocq, R., and Dumont, J.E. (1989). Protein synthesis during induction of DNA replication in thyroid epithelial cells: evidence for late markers of distinct mitogenic pathways. J. Cell. Physiol. *138*, 568–578. https://doi.org/10.1002/jcp.1041380318.

46. Baptist, M., Dumont, J.E., and Roger, P.P. (1993). Demonstration of cell cycle kinetics in thyroid primary culture by immunostaining of proliferating cell nuclear antigen: differences in cyclic AMP-dependent and -independent mitogenic stimulations. J. Cell Sci. *105*, 69–80. https://doi.org/10.1242/jcs.105.1.69.

47. Coulonval, K., Vandeput, F., Stein, R.C., Kozma, S.C., Lamy, F., and Dumont, J.E. (2000). Phosphatidylinositol 3-kinase, protein kinase B and ribosomal S6 kinases in the stimulation of thyroid epithelial cell proliferation by cAMP and growth factors in the presence of insulin. Biochem. J. *348*, 351–358. https://doi.org/10.1042/bj3480351.

48. Ciullo, I., Diez-Roux, G., Di Domenico, M., Migliaccio, A., and Avvedimento, E.V. (2001). cAMP signaling selectively influences Ras effectors pathways. Oncogene *20*, 1186–1192. https://doi.org/10.1038/sj.onc.1204219.

49. Cass, L.A., Summers, S.A., Prendergast, G.V., Backer, J.M., Birnbaum, M.J., and Meinkoth, J.L. (1999). Protein kinase A-dependent and -independent signaling pathways contribute to cyclic AMP-stimulated proliferation. Mol. Cell Biol. *19*, 5882–5891. https://doi.org/10.1128/mcb.19.9.5882.

50. Medina, D.L., Toro, M.J., and Santisteban, P. (2000). Somatostatin interferes with thyrotropin-induced G1-S transition mediated by cAMP-dependent protein kinase and phosphatidylinositol 3-kinase. Involvement of RhoA and cyclin E x cyclin-dependent kinase 2 complexes. J. Biol. Chem. *275*, 15549–15556. https://doi.org/10.1074/jbc.275.20.15549.

51. Dremier, S., Vandeput, F., Zwartkruis, F.J., Bos, J.L., Dumont, J.E., and Maenhaut, C. (2000). Activation of the small G protein Rap1 in dog thyroid cells by both cAMP-dependent and -independent pathways. Biochem. Biophys. Res. Commun. *267*, 7–11. https://doi.org/10.1006/bbrc.1999.1919.

52. Tsygankova, O.M., Saavedra, A., Rebhun, J.F., Quilliam, L.A., and Meinkoth, J.L. (2001). Coordinated regulation of Rap1 and thyroid differentiation by cyclic AMP and protein kinase A. Mol. Cell Biol. *21*, 1921–1929. https://doi.org/10.1128/mcb.21.6.1921-1929.2001.

53. Vossler, M.R., Yao, H., York, R.D., Pan, M.G., Rim, C.S., and Stork, P.J. (1997). cAMP activates MAP kinase and Elk-1 through a B-Raf- and Rap1-dependent pathway. Cell *89*, 73–82. https://doi.org/10.1016/s0092-8674(00)80184-1.

54. Iacovelli, L., Capobianco, L., Salvatore, L., Sallese, M., D'Ancona, G.M., and De Blasi, A. (2001). Thyrotropin activates mitogen-activated protein kinase pathway in FRTL-5 by a cAMP-dependent protein kinase A-independent mechanism. Mol. Pharmacol. *60*, 924–933. https://doi.org/10.1124/mol.60.5.924.

55. Chakravarty, D., Santos, E., Ryder, M., Knauf, J.A., Liao, X.H., West, B.L., Bollag, G., Kolesnick, R., Thin, T.H., Rosen, N., et al. (2011). Small-molecule MAPK inhibitors restore radioiodine incorporation in mouse thyroid cancers with conditional BRAF activation. J. Clin. Invest. *121*, 4700–4711. https://doi.org/10.1172/jci46382.

56. Maier, J., van Steeg, H., van Oostrom, C., Karger, S., Paschke, R., and Krohn, K. (2006). Deoxyribonucleic acid damage and spontaneous mutagenesis in the thyroid gland of rats and mice. Endocrinology *147*, 3391–3397. https://doi.org/10.1210/en.2005-1669.

57. Ziros, P.G., Chartoumpekis, D.V., Georgakopoulos-Soares, I., Psarias, G., and Sykiotis, G.P. (2024). Transcriptomic profiling of the response to excess iodide in Keap1 hypomorphic mice reveals new gene-environment interactions in thyroid homeostasis. Redox Biol. *69*, 102978. https://doi.org/10.1016/j.redox.2023.102978.

58. Teshiba, R., Tajiri, T., Sumitomo, K., Masumoto, K., Taguchi, T., and Yamamoto, K. (2013). Identification of a KEAP1 germline mutation in a family with multinodular goitre. PLoS One *8*, e65141. https://doi.org/10.1371/journal.pone.0065141.

59. Nishihara, E., Hishinuma, A., Kogai, T., Takada, N., Hirokawa, M., Fukata, S., Ito, M., Yabuta, T., Nishikawa, M., Nakamura, H., et al. (2016). A Novel Germline Mutation of KEAP1 (R483H) Associated with a Non-Toxic Multinodular Goiter. Front. Endocrinol. *7*, 131. https://doi.org/10.3389/fendo.2016.00131.

60. Ziros, P.G., Renaud, C.O., Chartoumpekis, D.V., Bongiovanni, M., Habeos, I.G., Liao, X.H., Refetoff, S., Kopp, P.A., Brix, K., and Sykiotis, G.P. (2021). Mice Hypomorphic for Keap1, a Negative Regulator of the Nrf2 Antioxidant Response, Show Age-Dependent Diffuse Goiter with Elevated Thyrotropin Levels. Thyroid *31*, 23–35. https://doi.org/10.1089/thy.2020.0044.

61. Ugradar, S., Malkhasyan, E., and Douglas, R.S. (2024). Teprotumumab for the treatment of Thyroid eye disease. Endocr. Rev. *45*, 843–857. https://doi.org/10.1210/endrev/bnae018.

62. Lin, Q., Qi, Q., Hou, S., Chen, Z., Jiang, N., Zhang, L., and Lin, C. (2021). Activation of the TGF-β1/Smad signaling by KIF2C contributes to the malignant phenotype of thyroid carcinoma cells. Tissue. Cell *73*, 101655. https://doi.org/10.1016/j.tice.2021.101655.

63. Wu, Y., Chen, W., Miao, H., and Xu, T. (2024). SIRT7 promotes the proliferation and migration of anaplastic thyroid cancer cells by regulating the desuccinylation of KIF23. BMC Cancer *24*, 210. https://doi.org/10.1186/s12885-024-11965-9.

64. D'Amico, E., Gayral, S., Massart, C., Van Sande, J., Reiter, J.F., Dumont, J.E., Robaye, B., and Schurmans, S. (2013). Thyroid-specific inactivation of KIF3A alters the TSH signaling pathway and leads to hypothyroidism. J. Mol. Endocrinol. *50*, 375–387. https://doi.org/10.1530/jme-12-0219.

65. Abuid, J., and Larsen, P.R. (1974). Triiodothyronine and thyroxine in hyperthyroidism. Comparison of the acute changes during therapy with antithyroid agents. J. Clin. Invest. *54*, 201–208. https://doi.org/10.1172/jci107744.

66. Pekary, A.E., Berg, L., Santini, F., Chopra, I., and Hershman, J.M. (1994). Cytokines modulate type I iodothyronine deiodinase mRNA levels and enzyme activity in FRTL-5 rat thyroid cells. Mol. Cell. Endocrinol. *101*, R31–R35. https://doi.org/10.1016/0303-7207(94)90256-9.

67. Gereben, B., Salvatore, D., Harney, J.W., Tu, H.M., and Larsen, P.R. (2001). The human, but not rat, dio2 gene is stimulated by thyroid transcription factor-1 (TTF-1). Mol. Endocrinol. *15*, 112–124. https://doi.org/10.1210/mend.15.1.0579.

68. Pesce, L., Bizhanova, A., Caraballo, J.C., Westphal, W., Butti, M.L., Comellas, A., and Kopp, P. (2012). TSH regulates pendrin membrane abundance and enhances iodide efflux in thyroid cells. Endocrinology *153*, 512–521. https://doi.org/10.1210/en.2011-1548.

69. Royaux, I.E., Suzuki, K., Mori, A., Katoh, R., Everett, L.A., Kohn, L.D., and Green, E.D. (2000). Pendrin, the protein encoded by the Pendred syndrome gene (PDS), is an apical porter of iodide in the thyroid and is regulated by thyroglobulin in FRTL-5 cells. Endocrinology *141*, 839–845. https://doi.org/10.1210/endo.141.2.7303.

70. Dentice, M., Luongo, C., Elefante, A., Ambrosio, R., Salzano, S., Zannini, M., Nitsch, R., Di Lauro, R., Rossi, G., Fenzi, G., and Salvatore, D. (2005). Pendrin is a novel *in vivo* downstream target gene of the TTF-1/Nkx-2.1 homeodomain transcription factor in differentiated thyroid cells. Mol. Cell Biol. *25*, 10171–10182. https://doi.org/10.1128/mcb.25.22.10171-10182.2005.

71. Mian, C., Lacroix, L., Alzieu, L., Nocera, M., Talbot, M., Bidart, J.M., Schlumberger, M., and Caillou, B. (2001). Sodium iodide symporter and pendrin expression in human thyroid tissues. Thyroid *11*, 825–830. https://doi.org/10.1089/105072501316973073.

72. Kondo, T., Nakamura, N., Suzuki, K., Murata, S.i., Muramatsu, A., Kawaoi, A., and Katoh, R. (2003). Expression of human pendrin in diseased thyroids. J. Histochem. Cytochem. *51*, 167–173. https://doi.org/10.1177/002215540305100205.

73. Smanik, P.A., Liu, Q., Furminger, T.L., Ryu, K., Xing, S., Mazzaferri, E.L., and Jhiang, S.M. (1996). Cloning of the human sodium lodide symporter. Biochem. Biophys. Res. Commun. *226*, 339–345. https://doi.org/10.1006/bbrc.1996.1358.

74. Iosco, C., Cosentino, C., Sirna, L., Romano, R., Cursano, S., Mongia, A., Pompeo, G., di Bernardo, J., Ceccarelli, C., Tallini, G., and Rhoden, K.J. (2014). Anoctamin 1 is apically expressed on thyroid follicular cells and contributes to ATP- and calcium-activated iodide efflux. Cell. Physiol. Biochem. *34*, 966–980. https://doi.org/10.1159/000366313.

75. Cangul, H., Liao, X.H., Schoenmakers, E., Kero, J., Barone, S., Srichomkwun, P., Iwayama, H., Serra, E.G., Saglam, H., Eren, E., et al. (2018). Homozygous loss-of-function mutations in SLC26A7 cause goitrous congenital hypothyroidism. JCI Insight *3*, e99631. https://doi.org/10.1172/jci.insight.99631.

76. Yamaguchi, N., Suzuki, A., Yoshida, A., Tanaka, T., Aoyama, K., Oishi, H., Hara, Y., Ogi, T., Amano, I., Kameo, S., et al. (2022). The iodide transporter Slc26a7 impacts thyroid function more strongly than Slc26a4 in mice. Sci. Rep. *12*, 11259. https://doi.org/10.1038/s41598-022-15151-4.

77. Montminy, M.R., and Bilezikjian, L.M. (1987). Binding of a nuclear protein to the cyclic-AMP response element of the somatostatin gene. Nature *328*, 175–178. https://doi.org/10.1038/328175a0.

78. Gonzalez, G.A., Yamamoto, K.K., Fischer, W.H., Karr, D., Menzel, P., Biggs, W., 3rd, Vale, W.W., and Montminy, M.R. (1989). A cluster of phosphorylation sites on the cyclic AMP-regulated nuclear factor CREB predicted by its sequence. Nature *337*, 749–752. https://doi.org/10.1038/337749a0.

79. Wiseman, S.M., Melck, A., Masoudi, H., Ghaidi, F., Goldstein, L., Gown, A., Jones, S.J.M., and Griffith, O.L. (2008). Molecular phenotyping of thyroid tumors identifies a marker panel for differentiated thyroid cancer diagnosis. Ann. Surg Oncol. *15*, 2811–2826. https://doi.org/10.1245/s10434-008-0034-8.

80. Iglesias, P., Silvestre, R.A., and Díez, J.J. (2023). Growth differentiation factor 15 (GDF-15) in endocrinology. Endocrine *81*, 419–431. https://doi.org/10.1007/s12020-023-03377-9.

81. Zhao, J., Li, M., Chen, Y., Zhang, S., Ying, H., Song, Z., Lu, Y., Li, X., Xiong, X., and Jiang, J. (2018). Elevated Serum Growth Differentiation Factor 15 Levels in Hyperthyroid Patients. Front. Endocrinol. *9*, 793. https://doi.org/10.3389/fendo.2018.00793.

82. Kang, Y.E., Kim, J.M., Lim, M.A., Lee, S.E., Yi, S., Kim, J.T., Oh, C., Liu, L., Jin, Y., Jung, S.N., et al. (2021). Growth Differentiation Factor 15 is a Cancer Cell-Induced Mitokine That Primes Thyroid Cancer Cells for Invasiveness. Thyroid *31*, 772–786. https://doi.org/10.1089/thy.2020.0034.

83. Hashimoto, K., Nishihara, E., Matsumoto, M., Matsumoto, S., Nakajima, Y., Tsujimoto, K., Yamakage, H., Satoh-Asahara, N., Noh, J.Y., Ito, K., et al. (2018). Sialic Acid-Binding Immunoglobulin-Like Lectin1 as a Novel Predictive Biomarker for Relapse in Graves' Disease: A Multicenter Study. Thyroid *28*, 50–59. https://doi.org/10.1089/thy.2017.0244.

84. Tona, Y., Sakamoto, T., Nakagawa, T., Adachi, T., Taniguchi, M., Torii, H., Hamaguchi, K., Kitajiri, S.i., and Ito, J. (2014). In vivo imaging of mouse cochlea by optical coherence tomography. Otol. Neurotol. *35*, e84–e89. https://doi.org/10.1097/mao.0000000000000252.

85. Everett, L.A., Belyantseva, I.A., Noben-Trauth, K., Cantos, R., Chen, A., Thakkar, S.I., Hoogstraten-Miller, S.L., Kachar, B., Wu, D.K., and Green, E.D. (2001). Targeted disruption of mouse Pds provides insight about the inner-ear defects encountered in Pendred syndrome. Hum. Mol. Genet. *10*, 153–161. https://doi.org/10.1093/hmg/10.2.153.

86. Yamauchi, I., Sakane, Y., Okuno, Y., Sugawa, T., Hakata, T., Fujita, H., Okamoto, K., Taura, D., Yamashita, T., Hirota, K., et al. (2022). High-throughput Screening in Combination With a Cohort Study for Iodothyronine Deiodinases. Endocrinology *163*, bqac090. https://doi.org/10.1210/endocr/bqac090.

STAR★METHODS

KEY RESOURCES TABLE

REAGENT or RESOURCE	SOURCE	IDENTIFIER
Antibodies		
Rabbit polyclonal anti-SLC26A4 antibody	Thermo Fisher Scientific	Cat# PA5-115911
Rabbit polyclonal anti-β-actin antibody	Cell Signaling Technology	Cat# 4967
Horseradish-peroxidase-conjugated goat polyclonal anti-rabbit IgG antibody	Southern Biotech	Cat# 4050-05
Chemicals, peptides, and recombinant proteins		
Sterilized saline	Otsuka Pharmaceutical Factory	YJ# 3311400A1068
2-Mercapto-1-methylimidazole (Thiamazole, MMI)	Tokyo Chemical Industry Co., Ltd.	Cat# P0533
6-propyl-2-thiouracil (Propylthiouracil, PTU)	Tokyo Chemical Industry Co., Ltd.	Cat# M0868
RNAprotect Tissue Reagent	QIAGEN	Cat# 76104
4% paraformaldehyde phosphate buffer solution	FUJIFILM Wako Pure Chemical Corporation	Cat# 163-20145
Radioimmunoprecipitation buffer	Nacalai Tesque	Cat# 08714-04
Methanol	Nacalai Tesque	Cat# 21914
Chloroform	Nacalai Tesque	Cat# 08401
Protein Assay CBB Solution	Nacalai Tesque	Cat# 29449
Bovine serum albumin	Bio-Rad	Cat# 5000206
Bullet Blocking One	Nacalai Tesque	Cat# 13779
Chemi-Lumi One Super	Nacalai Tesque	Cat# 02230
Critical commercial assays		
NucleoBond Xtra Midi Plus kit	Macherey-Nagel	Cat# 740412
FT3, FT4, TSH AccuLite VAST CLIA kit	Monobind Inc.	Cat# 7075
cAMP-Glo™ Max Assay	Promega	Cat# V1681
Nucleospin RNA Plus kit	Macherey-Nagel	Cat# 740984
ReverTra Ace	TOYOBO Life Science	Cat# FSQ-201
Emerald Amp MAX PCR master mix	Takara Bio	Cat# RR320A
THUNDERBIRD SYBR qPCR MIX	TOYOBO Life Science	Cat# QPS-201
TruSeq Stranded mRNA Sample Prep Kit	Illumina	Cat# 20020595
Experimental models: Organisms/strains		
C57BL/6J mice	Japan SLC, Inc.	N/A
Slc26a4 knockout mice in C57BL/6J background	This paper	N/A
Deposited data		
RNA sequence data	This paper	GEO# GSE279577
Oligonucleotides		
Primers used for plasmid construction, RT-PCR, and quantitative RT-PCR	This paper	See Table S10
Recombinant DNA		
pLIVE-Empty	Mirus Bio	Cat# MIR5420
pLIVE-*TSHB*	This paper	N/A
pLIVE-*CGA*	This paper	N/A
Software and algorithms		
ImageJ	National Institutes of Health	https://imagej.nih.gov/ij/
JMP Pro version 17.0.0	SAS Institute Inc.	https://www.jmp.com/
Other		
27-gauge needle	Terumo Corporation	Cat# SV-S27EL

(*Continued on next page*)

Continued

REAGENT or RESOURCE	SOURCE	IDENTIFIER
Nanodrop-1000 spectrophotometer	Thermo Fisher Scientific	https://www.thermofisher.com/
2030 ARVO X3 multilabel reader	PerkinElmer	https://content.perkinelmer.com/
Spark	Tecan	https://lifesciences.tecan.com/multimode-plate-reader
Speed Vac™ DNA 110 Concentrator	Savant	https://www.thermofisher.com/
StepOnePlus Real-Time PCR	Thermo Fisher Scientific	Cat# 4376598
NovaSeq 6000 system	Illumina	Cat# 20012850
Bolt 4–12% Bis-Tris Plus Gels	Thermo Fisher Scientific	Cat# NW04122BOX
ImageQuant LAS 4000	GE Healthcare	Cat# LAS-4000

EXPERIMENTAL MODEL AND STUDY PARTICIPANT DETAILS

Animals

We purchased male C57BL/6J mice from Japan SLC, Inc. (Hamamatsu, Japan). In the present study, *Slc26a4* knockout mice[84,85] were backcrossed with C57BL/6J mice. All experimental procedures involving animals were approved by the Animal Research Committee of the Kyoto University Graduate School of Medicine (approval number, Med Kyo 19512). Animal care and all animal experiments were conducted in accordance with our institutional guidelines. All animals were housed at 23°C in a 14:10–hour light/dark cycle.

METHOD DETAILS

Plasmid construction

We cloned the coding sequences of human *TSHB* and *CGA* into pLIVE vectors (Mirus Bio, Madison, WI) using a polymerase chain reaction (PCR) technique with primers containing restriction enzyme sites and the Kozak sequence (Table S10). The constructed vectors were verified based on sequencing. We prepared a large amount of these plasmid vectors using a NucleoBond Xtra Midi Plus kit (Macherey-Nagel, Düren, Germany). Concentrations of plasmid DNA were measured with a Nanodrop-1000 spectrophotometer (Thermo Fisher Scientific, Waltham, MA).

Hydrodynamic gene delivery and MMI administration

Six-week-old male C57BL/6J mice were injected with 50 μg of pLIVE-Empty vector or a mixture of 25 μg of pLIVE-*TSHB* vector and 25 μg of pLIVE-*CGA* vector using a hydrodynamic gene delivery method, as in our previous studies.[25–27] Briefly, a solution of plasmid DNA and sterilized saline (Otsuka Pharmaceutical Factory, Tokyo, Japan) was prepared as a total volume equivalent to 8–10% of the weight of each mouse. The solution was rapidly injected within 10 seconds into the tail vein using a 27-gauge needle (Terumo Corporation, Tokyo, Japan). Male *Slc26a4* knockout mice were injected with 100 μg of pLIVE-Empty vector or a mixture of 50 μg of pLIVE-*TSHB* vector and 50 μg of pLIVE-*CGA* vector at 6 weeks of age. Regarding administration of MMI (Tokyo Chemical Industry Co., Ltd., Tokyo Japan), mice had *ad libitum* access to drinking water containing 20 μg/mL of MMI without sweeteners. PTU (Tokyo Chemical Industry Co., Ltd.) was administered in a similar manner. In the experiment related to Figure S8, we prepared drinking water containing 200 μg/mL of either MMI or PTU.

Sample collection

At 1 day, 3 days, 1 week, or 4 weeks after hydrodynamic gene delivery, we sacrificed the mice and collected samples. All mice were sacrificed using isoflurane exposure at the end of the light cycle, except for the experiment related to Figure S2. To obtain serum, blood samples were collected in microtubes and left undisturbed for 45 minutes at room temperature. Next, these samples were left on ice and immediately centrifuged at 3,000 g for 15 minutes at 4°C. The supernatants were collected and stored at −80°C until use. Thyroid glands and pituitary glands harvested for RNA extraction were preserved in RNAprotect Tissue Reagent (QIAGEN, Venlo, Netherlands) at −20°C until use. Thyroid glands harvested for histological analyses were first fixed in 4% paraformaldehyde phosphate buffer solution (FUJIFILM Wako Pure Chemical Corporation, Osaka, Japan), embedded in paraffin, and stained using hematoxylin and eosin. Thyroid glands harvested for western blotting analyses were collected in microtubes, immediately frozen in liquid nitrogen, and stored at −80°C until use.

Thyroid morphological analysis

Morphological analysis of thyroid glands was performed using ImageJ software (National Institutes of Health, Bethesda, MD) as follows. Thyroid gland size was measured as thyroid area on the photograph. Thyroid follicle size was measured using histological

images at 50X magnification. The area of the thyroid gland was trimmed, converted to grayscale, and underwent black and white inversion. Particle analyses were performed on the processed images. Values greater than 500 μm^2 were used. For each mouse, we evaluated the right and left lobes and calculated the average value. Follicular epithelial cell height was measured on histological images at 200X magnification. Heights at the upper, bottom, right, and left sides of follicles were measured. The average height from 5 follicles was calculated.

Measurement of thyroid hormones and cAMP

Serum levels of fT3, fT4, and human TSH were measured using a FT3, FT4, TSH AccuLite VAST CLIA kit (Monobind Inc., Lake Forest, CA). We diluted serum samples 25-fold with phosphate buffered saline when we measured human TSH levels. Luminescence was measured using a 2030 ARVO X3 multilabel reader (PerkinElmer, Waltham, MA) or multilevel reader Spark (Tecan, Zurich, Switzerland).

We mechanically homogenized the thyroid gland of a mouse in 200 μL of radioimmunoprecipitation buffer (Nacalai Tesque, Kyoto, Japan) and left them on ice for 30 minutes. The supernatants were centrifuged at 10 000 g for 10 min at 4°C and collected in microtubes. We added 200 μL of methanol (Nacalai Tesque) and 400 μL of chloroform (Nacalai Tesque), vortexed, and centrifuged at 15 000 g for 2 minutes at 4°C. The upper water/methanol phase was collected in new microtubes and dried using a Speed Vac™ DNA 110 Concentrator (Savant, Farmingdale, NY, USA). The pellets were suspended in phosphate-buffered saline. T3 and T4 concentrations were determined using a FT3, FT4, and TSH AccuLite VAST CLIA kit, and cAMP concentrations were using cAMP-Glo™ Max Assay (Promega, Madison, WI, USA). Protein concentrations of lysates were evaluated using the Bradford method with Protein Assay CBB Solution (Nacalai Tesque); bovine serum albumin (Bio-Rad, Hercules, CA) was used as the standard.

RNA extraction, RT-PCR, and quantitative RT-PCR

Total RNA was extracted using a Nucleospin RNA Plus kit (Macherey-Nagel) according to the manufacturer's instructions. All extracted RNA was reverse transcribed using ReverTra Ace (TOYOBO Life Science, Osaka, Japan). Reverse transcription (RT)-PCR was performed using the Emerald Amp MAX PCR master mix (Takara Bio, Shiga, Japan). Quantitative RT-PCR was performed using THUNDERBIRD SYBR qPCR MIX (TOYOBO Life Science) with the StepOnePlus Real-time PCR System (Thermo Fisher Scientific), as in our previous studies.[26,27,34,86] Results were normalized using *Ppia* and *Hprt* as reference genes; relative mRNA expression of target genes was evaluated using the comparative threshold cycle method. Table S10 lists the primers used.

RNA-seq and bioinformatics analysis

The TruSeq Stranded mRNA Sample Prep Kit (Illumina, Inc., San Diego, CA) was used to construct mRNA paired-end libraries. Paired-end sequencing of 100 bp was performed on an NovaSeq 6000 system (Illumina, Inc.). Quality control metrics of raw sequencing reads were performed with FastQC version 0.11.7; low-quality reads were removed with Trimmomatic version 0.38. Next, reads were mapped to the mm10 reference sequence with HISAT2 version 2.1.0 and assembled into transcripts with StringTie version 2.1.3b. The expression profile was calculated as transcripts per kilobase million. For DEG analyses, fold change values were calculated and DEGs with an adjusted $p < 0.05$ and fold changes ≤ -2 or ≥ 2 were determined using DESeq2. Gene-set enrichment analyses were performed based on GO with gProfiler and the KEGG database. These experiments and analyses were conducted by Macrogen Japan (Tokyo, Japan).

Western blotting

We mechanically homogenized a lobe of the thyroid gland in 100 μL radioimmunoprecipitation buffer (Nacalai Tesque) and left the homogenate on ice for 30 minutes. Supernatants were centrifuged at 10,000 *g* for 10 minutes at 4°C and collected in microtubes. Protein concentrations were evaluated using the Bradford method with bovine serum albumin as the standard. We performed electrophoresis with 20 μg/lane of each lysate in Bolt 4–12% Bis-Tris Plus Gels (Thermo Fisher Scientific). We transferred the protein samples onto polyvinylidene difluoride membranes with the iBlot2 Dry Blotting System (Thermo Fisher Scientific). The membranes were blocked with Bullet Blocking One (Nacalai Tesque). We incubated with primary antibodies overnight at 4°C followed by secondary antibodies for 2 hours at room temperature. Bands were detected using a chemiluminescent method with Chemi-Lumi One Super (Nacalai Tesque) in ImageQuant LAS 4000 (GE Healthcare, Chicago, IL). The primary antibody was a rabbit polyclonal anti-SLC26A4 antibody (PA5-115911; Thermo Fisher Scientific). A rabbit polyclonal anti-β-actin antibody (4967; Cell Signaling Technology, Danvers, MA) was used as the endogenous control. The secondary antibody was a horseradish-peroxidase-conjugated goat polyclonal anti-rabbit IgG antibody (4050-05; Southern Biotech, Cambridge, United Kingdom).

QUANTIFICATION AND STATISTICAL ANALYSIS

All results are expressed as means ± standard error of the mean. Student's *t*-test or one-way analysis of variance followed by the Dunnett test or the Tukey-Kramer test was used to analyze data on mouse phenotypes. JMP Pro version 17.0.0 (SAS Institute Inc., Cary, NC) was used for statistical analysis. Statistical analyses of DEGs were performed with the Wald test using DESeq2. Fisher's exact test was used for enrichment analyses. Statistical significance was defined as $p < 0.05$.